STUDY OF THE LOW ENERGY CHARGED PARTICLES EMITTED IN THE INTERACTION OF 6 BeV AND 27 BeV PROTONS WITH Ag AND Br NUCLEI.

by

Kendal R. Crouch

Submitted in partial fulfillment
of the requirements for the degree of
Master of Science.

Department of Physics,
Faculty of Pure and Applied Science,
The University of Ottawa,
Ottawa, Canada.

1965

Approved for the

Department of Physics

Supervisor

Chairman of the Examining Committee

Chairman of the Department

ABSTRACT

A study has been made of the low-energy charged particles emitted from the interactions of 6 BeV and 27 BeV protons with silver and bromine nuclei in nuclear emulsions. The energy spectra of the protons and α particles are compared with the Weisskopf evaporation theory and with experimental results at other bombarding energies. The evaporation temperatures of the excited nuclei were determined for the emission of protons (including deuterons and tritons) and α particles, respectively, for the two primary proton energies of 6 BeV and 27 BeV. The two proton energy spectra are consistent with an evaporation temperature of 4 to 5 MeV and a potential barrier $V' \sim 3\text{-}4$ MeV. For the α particle spectra, the parameters for the evaporation curves which give the best fit to the experimental distributions are a temperature, T, of the order of 10 to 12 MeV and a potential barrier V' very nearly equal to zero. These abnormally high temperatures (greater than the binding energy of a nucleon inside the nucleus) indicate that the emission process cannot be entirely explained in terms of a normal mechanism of evaporation from a thermodynamic equilibrium state. Applying the value of T obtained from the proton energy spectra, with a value of $V' \sim 7\text{-}8$ MeV, gives a satisfactory fit of the theoretical curve to the experimental distribution for α energies less

than 30 MeV.

A study of the angular distributions of the emitted α particles shows that the emission is anisotropic, the distribution being peaked in the forward direction; this peaking is more pronounced at 6 BeV than at 27 BeV. In both cases, the forward peaking appears to be due exclusively to α particles of energy greater than 30 MeV. We may conclude, therefore, that these higher-energy particles are probably associated with secondary interactions provoked by the cascade, rather than with the pure evaporation process.

In an attempt to understand the processes of interaction of 6 BeV protons with heavy nuclei, the angular distributions of the black tracks have been studied for stars previously analyzed in terms of the charged π-meson distribution. The results are discussed for the cases when the incident proton collides:

(a) with a single nucleon in the target nucleus, and

(b) with 3 to 5 target nucleons.

The results indicate that the interactions with a single target nucleon occur at the periphery of the nucleus, the two nucleons then leaving the nucleus without initiating a cascade. The star size and the average excitation energy are found to be smaller for the single nucleon interactions than in the case of the (3-4-5) target nucleon interactions and the probability of fragment emission appears to be greater.

ACKNOWLEDGMENTS

I wish to express my gratitude to Mr. Jacques Hébert, my supervisor, for his suggestion of this interesting research topic and for his able guidance and encouragement throughout.

I am grateful to Mrs. J. Hébert for her valuable assistance and for the keen interest shown in this work. In particular I wish to thank her for communicating to me, prior to publication, her measurements on low energy α particles.

I also wish to thank Mr. Sheung Tsing Lam whose measurements allowed completion of the third part of this work, as well as my fellow students, especially Mr. Hans Mes, for their interest and helpful discussions.

I am indebted to the Nuclear Emulsion groups from the National Research Council and the Institute for Theoretical Physics (Denmark) for supplying the nuclear emulsion plates.

Financial assistance through a National Research Council grant is also gratefully acknowledged.

TABLE OF CONTENTS

LIST OF ILLUSTRATIONS

LIST OF TABLES

INTRODUCTION

The low-energy particles emitted in the disintegration of emulsion nuclei bombarded by high-energy nucleons have been studied by many investigators[1-16]. The early studies[1-10] were made with non-monoenergetic bombarding particle sources (cosmic rays). In recent years, however, high-energy particle accelerators have provided mono-energetic sources[11-16] and incident particle energies of up to 30 BeV are now available.

The emulsion technique is particularly convenient for the study of interactions with complex nuclei, since silver and bromine constitute about 50% by volume of the normal sensitive emulsion. The interactions with the lighter constituents (hydrogen, carbon, nitrogen and oxygen) can be recognised from the number of black prongs (≤ 7) in the stars resulting from the disintegration of the struck nucleus. The exact processes involved in interactions with complex nuclei are not well known, although the general features of the mechanism have been demonstrated.

When a proton with an energy of a few BeV collides with a nucleus, energetic π-mesons, charged and uncharged, are produced. These mesons may escape from the nucleus with very little loss of kinetic energy, though they may produce other mesons as a result of further collisions with nucleons. The energetic charged mesons (and fast protons) resulting from the

initial impact, emerge from the nucleus to form shower tracks in the nuclear emulsion. A great many investigations[17-22] have been carried out on these shower particles. Analyses of the angular distributions of the mesons have shown that the incident particle can collide with different target masses when striking a nucleus.

The nucleons from the initial collision are frequently less energetic and may interact with other nucleons; these recoiling particles may interact in turn with more nucleons, and so on, producing a nucleon-cascade. Some of the recoiling protons may emerge from the nucleus, forming "grey" tracks in the emulsion. As a result of the nucleon cascade, the residual nucleus is left in a highly excited state. Emission of particles from this state takes place relatively slowly. A particle cannot escape until, as a result of random nuclear collisions, it is projected towards the nuclear boundary with a kinetic energy exceeding its binding energy. Before the emission of another particle, a long delay (on the nuclear time scale) will take place. The process has been likened to the cooling down of a liquid drop by the process of evaporation. However, the liquid drop model has been tested and found to be unsatisfactory[1]. At these high excitation energies, it seems reasonable to assume a free particle model for the excited nucleus. Evaporation theories based on the Fermi gas model have been developed by Weisskopf[23], and by Le Couteur[24].

The low-energy evaporated particles have high specific ionization and will form "black" tracks in the emulsion. In addition to low-energy protons, the black tracks will also include α particles and light fragments as well as the track of the recoiling residual nucleus.

In this work we try to investigate the secondary processes involved in the interactions of high-energy protons with heavy nuclei from a study of the black tracks in the stars produced in nuclear emulsion. It is of interest to see if there is any significant difference in the emission of the secondary protons and α particles as the bombarding energy is increased from 6 BeV to 27 BeV. Some workers[25] have noticed that the proton and α particle energy spectra show a long high-energy tail which is not consistent with evaporation theory[24]. From a study of the energy spectra for different primary proton energies, some insight into the mechanism of emission of these higher energy particles might be obtained.

In the third part of the work, we make an attempt to see how the emission of the low energy particles varies with the nature (or type) of the primary collision. In this investigation we use stars which have been identified as collisions of the primary proton either with one nucleon in the target nucleus or with (3-4-5) target nucleons, the classification being based on the angular distribution of the shower mesons[21,22].

In collisions with one nucleon at the periphery of the nucleus, the nucleon cascade is unlikely to develop and the subsequent de-excitation of the nucleus probably takes place solely by the evaporation process. In the collisions with larger target masses, secondary processes associated with the cascade may occur before an equilibrium state of the nucleus is reached.

PART I.

The Identification of Low-Energy Particles.

I. Classification of Tracks.

The tracks in the stars resulting from the interaction of high-energy particles with emulsion nuclei are usually divided into three categories based on the specific ionization of the emitted particle. The specific ionization is related directly to the grain density along the track and hence the classification is made in terms of the relative "blackness" of the track.

The grain density, g, corresponding to a particular value of the specific ionization depends on the sensitivity of the emulsion and on the degree of development. For a classification of tracks to be based on the grain density, it is therefore necessary to determine the ratio of the observed grain density, g, to the corresponding value, g_o, for the track of a particle, with a velocity in the extreme relativistic region, observed in the same emulsion. Such "normalisation" is best made by choosing a comparison track in the same region of the emulsion. In the present case, the most convenient comparison tracks are those of the incident high-energy protons. Although at 6 BeV, the grain density of the proton track has not quite reached the "plateau" value, it was considered sufficiently good for the present purposes of classification to determine the normalised grain density relative to the incident proton tracks.

The three categories of tracks are classified according to the values of the normalised grain densities as follows:

(a) shower tracks: $g/g_o \leq 1.4$

(b) grey tracks: $1.4 < g/g_o < 10$

(c) black tracks: $g/g_o \geq 10$

In the present study we are concerned only with the black tracks. The value of 10 for the lower limit of g/g_o in the classification of the black tracks was chosen so that all the emitted α-particles (and fragments) would be included in this group. A value of $g/g_o = 10$ for a proton corresponds to a range of about 3 mm and an energy of ~ 26 MeV. The tracks of less than 10 μ range were considered as being due to recoil nuclei, or heavy fragments, and were not included in the analysis.

II. Types of Nuclear Emulsion.

The types of nuclear emulsion plates at our disposal were Ilford G5 and K5 emulsions (14 cm x 10 cm x 0.06 cm), exposed to the 6.2 BeV proton beam from the Berkeley Bevatron, and one Ilford L4 emulsion plate (30 cm x 10 cm x 0.06 cm), exposed to the 27 BeV proton beam from the CERN proton synchrotron. The G5 and K5 plates were developed by Dr. B. Judek[26] at the National Research Council, Ottawa, while the processing of the L4 plate was carried out by Dr. E. Dahl-Jensen[27] at the Institute for Theoretical Physics of Copenhagen.

Since the main purpose of the present work is to compare the low-energy particles emitted in the interactions produced by 6 BeV and 27 BeV protons with silver and bromine nuclei, it was unfortunately not possible to carry out the whole study with the same type of emulsion. Calibration measurements carried out with the G5 and K5 plates showed that the K5 plates were more useful for the comparison of the 6 BeV interactions with the 27 BeV interactions recorded in the L4 emulsion.

For the second part of the work, the analysis is performed on stars for which the π-meson distribution had already been studied. These studies by Ancsin[21] and by Lam[22] were made in the G5 plates. It was, therefore, necessary to make use of the three different types of emulsion. The techniques for the identification of low-energy particles were, therefore, calibrated and compared in the three types of emulsion.

III. Calibration of Development with Depth in the Emulsion.

Any identification technique involving a measurement of the ionization of a particle will not be reliable if the development is not uniform throughout the whole depth of the emulsion. In the event of non-uniform development, the variation in grain density with depth must be exactly determined and an appropriate correction applied to each measurement.

As a means of testing the uniformity of development of the emulsions, the variation in average grain size with depth was determined for the three types of emulsion. Measurements of grain size were made on the grains along flat tracks of relativistic particles observed at various depths below the surface of the emulsion. For these measurements, an oil-immersion objective, 100 x magnification, was used in conjunction with a 12.5 x micrometer eyepiece.

The grain size was found to be smallest in the L4 emulsion and greatest in the G5. The variation in average grain size with depth is shown in Figure 1. The Ilford L4 plate shows almost uniform grain size throughout the whole depth, whereas the K5 and G5 plates show an increase in grain diameter near the top and bottom of the emulsion. In order to avoid these regions of non-uniform development, the stars analysed were chosen, as far as possible, in the centre of the emulsion and measurements were not carried out on tracks within the regions corresponding to 100 μ, in the unprocessed emulsion, from the top and bottom emulsion surfaces.

IV. Identification Techniques.

The identification of particles in nuclear emulsions is based primarily on consideration of energy losses suffered in collisions with atomic electrons and on Coulomb scattering experienced in collisions with atomic nuclei.

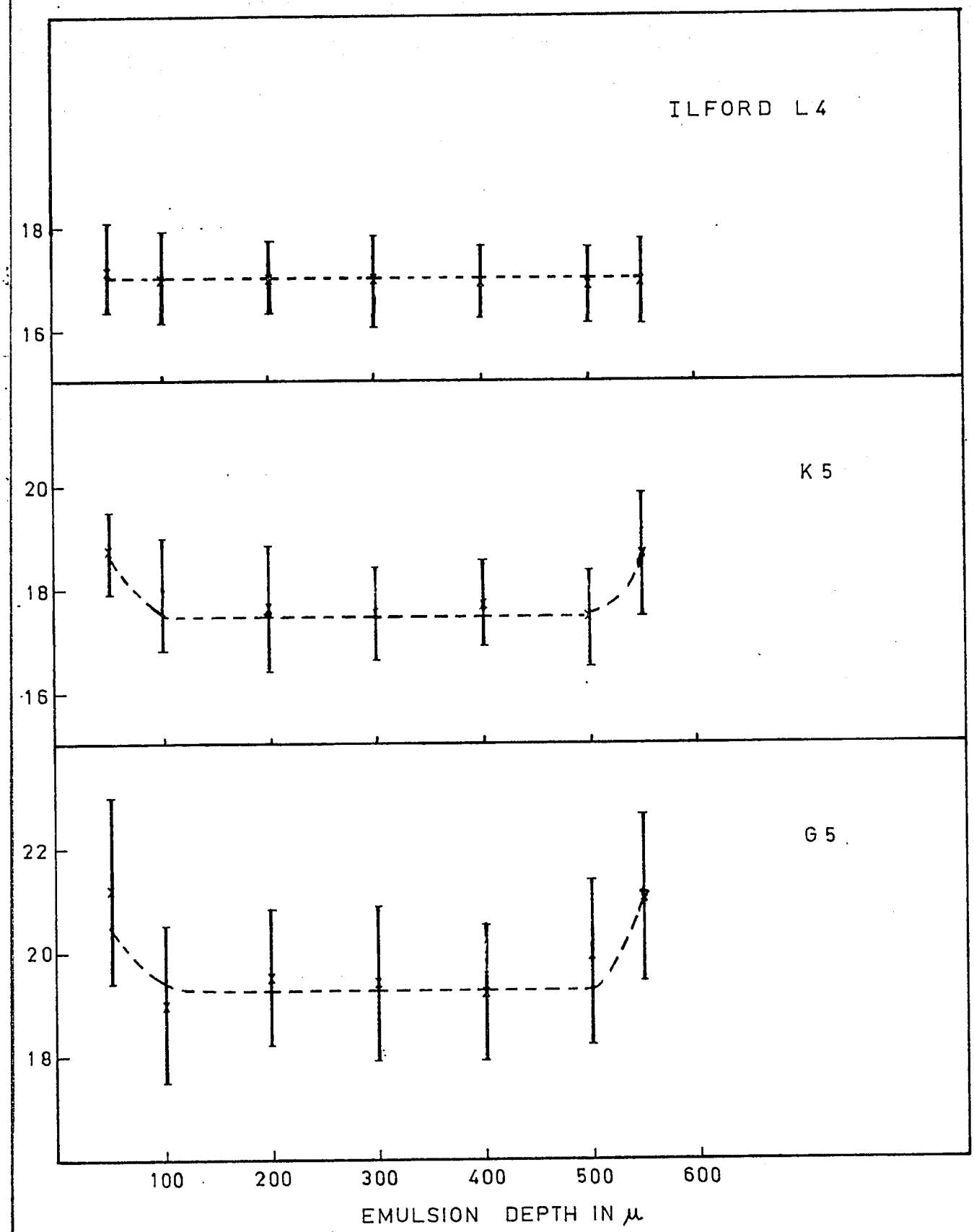

FIG. 1 DETERMINATION OF THE VARIATION OF GRAIN SIZE WITH DEPTH IN EMULSION FOR ILFORD L4, K5, G5

The interaction of the ionizing particle with atomic electrons may be separated as follows:

(a) Small energy transfers in which ions (primary ionization) are produced along the track. The emulsion grains rendered developable by these interactions form the central core of the track. A determination of the grain density or gap density along a track is a measure of this primary ionization.

(b) Larger energy transfers leading to the ejection of secondary electrons outside the initial grain of production and which may be sufficiently energetic to produce recognizable delta-ray tracks, or, if sufficiently numerous, may cause an appreciable thickening of the track.

Considerations of these interactions leads to the following methods of identification of low-energy particles, based on measurements of ionization along the track:

(a) grain, blob, or gap density along a track;

(b) linear density of delta-rays;

(c) measurements of track width.

The usefulness of each of these methods depends on the sensitivity and grain size of the emulsion used and on the degree of development, as well as on the charge of the ionizing particle.

Measurements of the Coulomb scattering along a track can be used to determine the mass and charge of a particle ending in the emulsion by a technique known as the "constant-sagitta" method. The identification is based on the determination of the

scattering of the particle at definite values of the residual range corresponding to cell-sizes for which the probable value of the sagitta of the scattering angle remains constant. In practice, the measurements are carried out by measuring the co-ordinates, in the plane of the emulsion, of a succession of points along the trajectory separated by a variable cell-length, t. The values of the cell-length are chosen in such a way that the probable value of the second differences of the y co-ordinates (which are proportional to the tangents of the scattering angles) is constant and equal to 0.5 μ for a proton. For any other singly charged particle of mass M, the arithmetic mean value $\bar{D}$ of the second differences is given, to a first approximation, by the relation

$$\frac{0.5}{\bar{D}} = \left(\frac{M}{M_p}\right)^{0.43}$$

Hence, the mass of the particle may be determined from the measured value of $\bar{D}$[28].

In the case where the particle does not end in the emulsion, the value of $\bar{D}$ for a constant cell-size is determined. The momentum, pβ, of a particle of charge Z is given by

$$p\beta = KZ/\bar{D},$$

where K is a constant which can be determined from the theoretical value of the scattering constant for a cell-length, t. Simultaneous measurements of pβ and the grain density can then

be used to determine the mass of the particle.

Thus, in addition to the techniques listed above, the following two methods of identification are available:

(d) range-scattering measurements,

and (e) ionization-scattering measurements.

The identification based on range-scattering measurements is not influenced by the sensitivity or the degree of development of the emulsion, but errors may be introduced if the emulsion shows distortion effects. The scattering measurements also suffer from the disadvantage of requiring long tracks in order to obtain a sufficiently accurate value of $\bar{D}$.

For the present study which is concerned with the identification of low-energy particles, the following techniques were found to be most useful:

(a) Range-scattering measurements.

(b) Linear density of low-energy delta-rays.

(c) Measurement of the tapering of a track near the end of its range.

(d) Gap counting.

V. Calibration of Plates.

(a) Delta Rays.

Rutherford's classical formula for the production of delta rays shows that the number of delta rays with kinetic energy between E and E + dE produced per unit range along the track of an ionizing particle is given by the relation

$$n(E)dE = \frac{2\pi N Z^2 e^4}{m_o c^2 \beta^2} \cdot \frac{dE}{E^2} \qquad (1)$$

Integrating, the number of δ rays per unit range of 100 μ is

$$\frac{n(\delta)}{100\mu} = k \frac{Z^2}{\beta^2} (1/E_o - 1/E_{max}) \qquad (2)$$

where

k is a constant;

N = the number of "free" electrons per unit volume of the target medium;

Z = atomic number of the ionizing particle;

e = electron charge;

m_o = electron rest mass;

c = velocity of light;

β = ratio of the velocity of incoming particle to the velocity of light;

and E_o and E_{max} are the minimum and maximum energies, in KeV, of the delta rays counted, corresponding of course to a given range which is chosen to suit experimental conditions. If no maximum limit is chosen, E_{max} is given by

$$E_{max} = \frac{2m_o c^2 \beta^2}{(1 - \beta^2)} \qquad (3)$$

Hence,

$$\frac{n\delta}{100\ \mu} = k\,\frac{Z^2}{\beta^2}\left[1/E_o - \frac{1-\beta^2}{2\,m_o c^2\,\beta^2}\right] \qquad (4)$$

Figure 2 shows the expected frequencies for several values of E_o. Characteristics of interest are:

a) A cut-off below a velocity β_1 given by

$$\beta_1^2 = E_o/(2m_o c^2 + E_o)$$

b) A maximum value at velocity β_2 given by

$$\frac{\partial}{\partial\beta}\ \frac{n(\delta)}{100\ \mu} = 0$$

Hence, $\beta_2^2 = \dfrac{E_o}{m_o c^2}$,

assuming that $m_o c^2 >> E_o$

c) A decrease with increasing velocity.

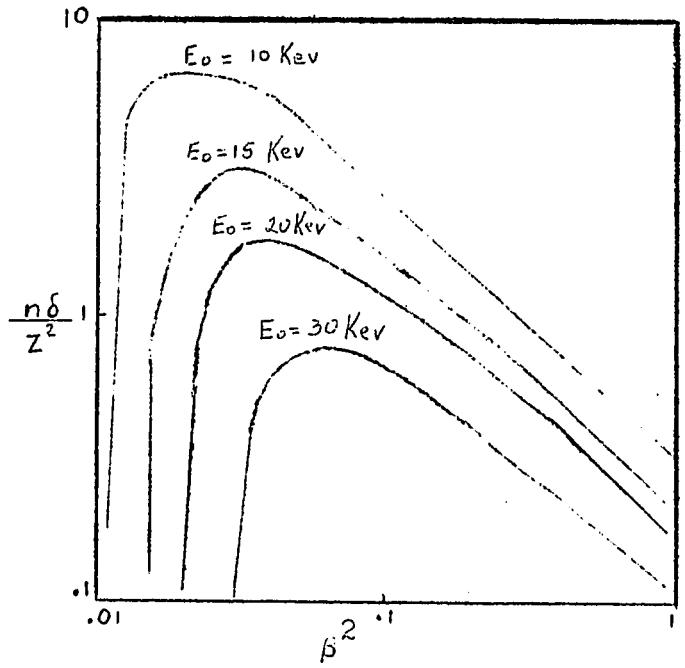

Figure 2: δ ray frequencies as a function of E_o, and β of primary.

Crussard[10] used a plot of $\frac{n\delta}{Z^2}$ as a function of R $\frac{Z^2}{A}$ (a function of β only), because R is an easier parameter to determine. The resulting curves have the same characteristic shape as those shown in Figure 2.

If this curve is plotted for protons whose tracks end in the emulsion (the protons having been identified by scattering-range measurements), the maximum number of delta rays per 100 microns can be determined. Since this curve can be used as a universal curve, this maximum can be determined for alpha particles and particles of higher Z as well. This characteristic maximum separates protons and α particle tracks not ending in the emulsion and, if a sufficient length of track is available, allows a minimum estimate of the charge of light fragments.

These calibration curves were obtained experimentally for Ilford L-4, K-5 and G-5 emulsions and the results are shown in Figure 3.

For tracks ending in the emulsion, the identification process is much simpler. In this case integral curves giving the total number of delta rays greater than one micron, as a function of the residual range, are plotted. It can easily be seen that these curves, plotted for protons, are universal curves applicable to particles of higher Z if the reduced range $R\frac{Z^2}{A}$ is plotted as abscissa and $\frac{N}{A}$ is plotted as ordinate. N is the total number of delta rays whose range is greater than 1 micron.

$$N = \int_o^R n dR = A\int \frac{n}{Z^2} dR \frac{Z^2}{A}$$

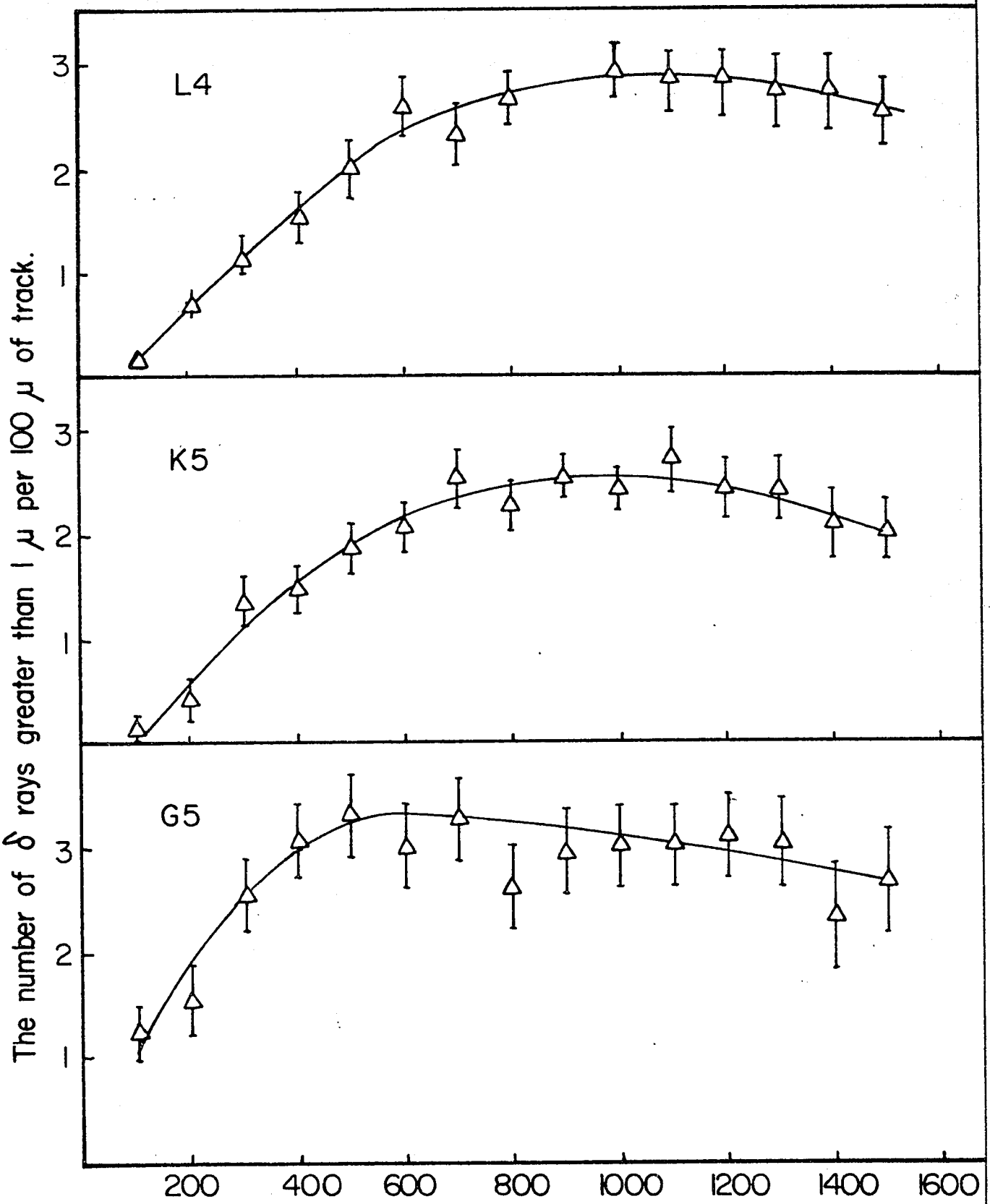

Fig. 3 Linear density of δ rays for proton tracks in Ilford L4, K5, G5 emulsions.

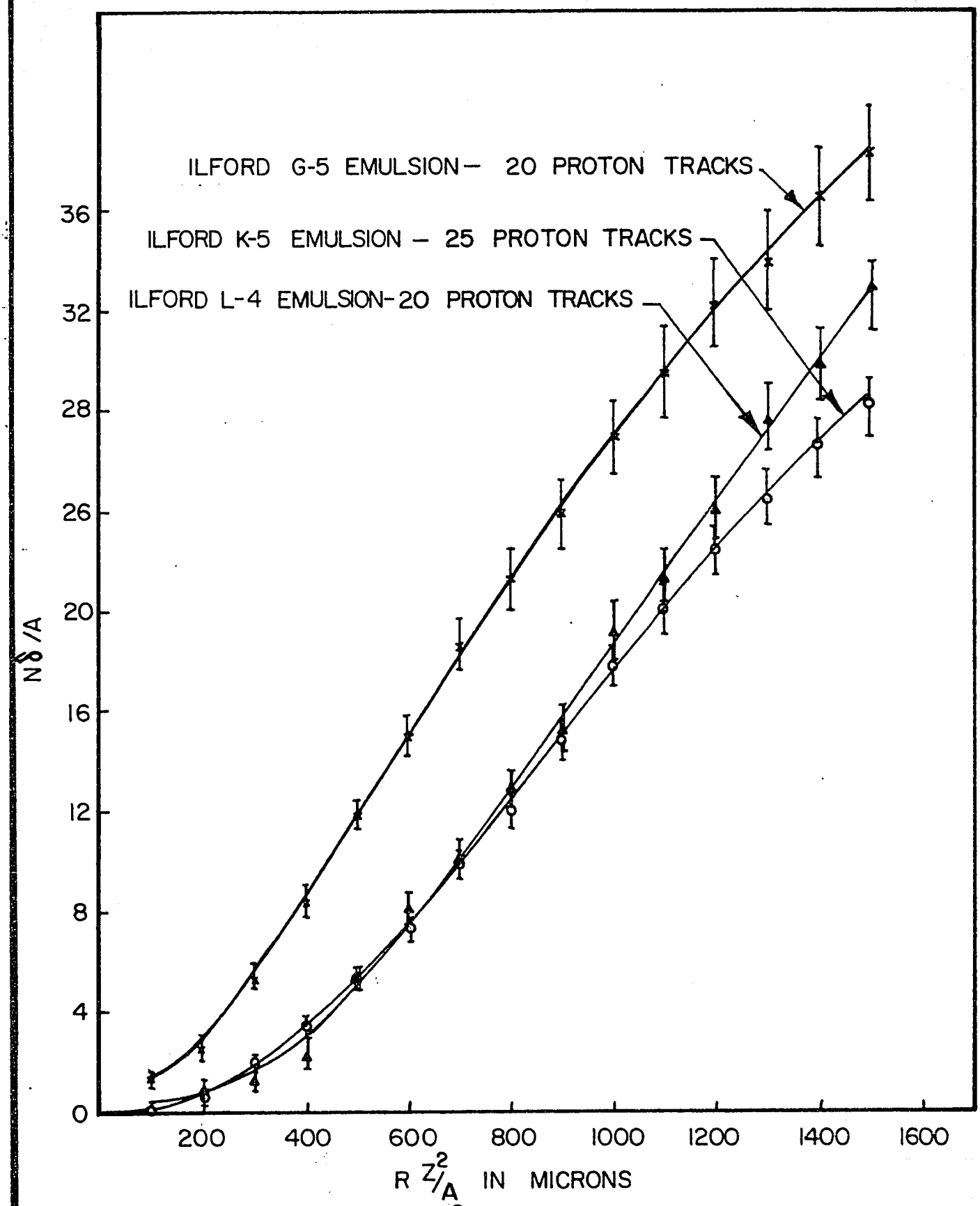

FIG. 4 PLOT OF $N\delta/A$ VS $R\,Z^2/A$ FOR PROTON TRACKS

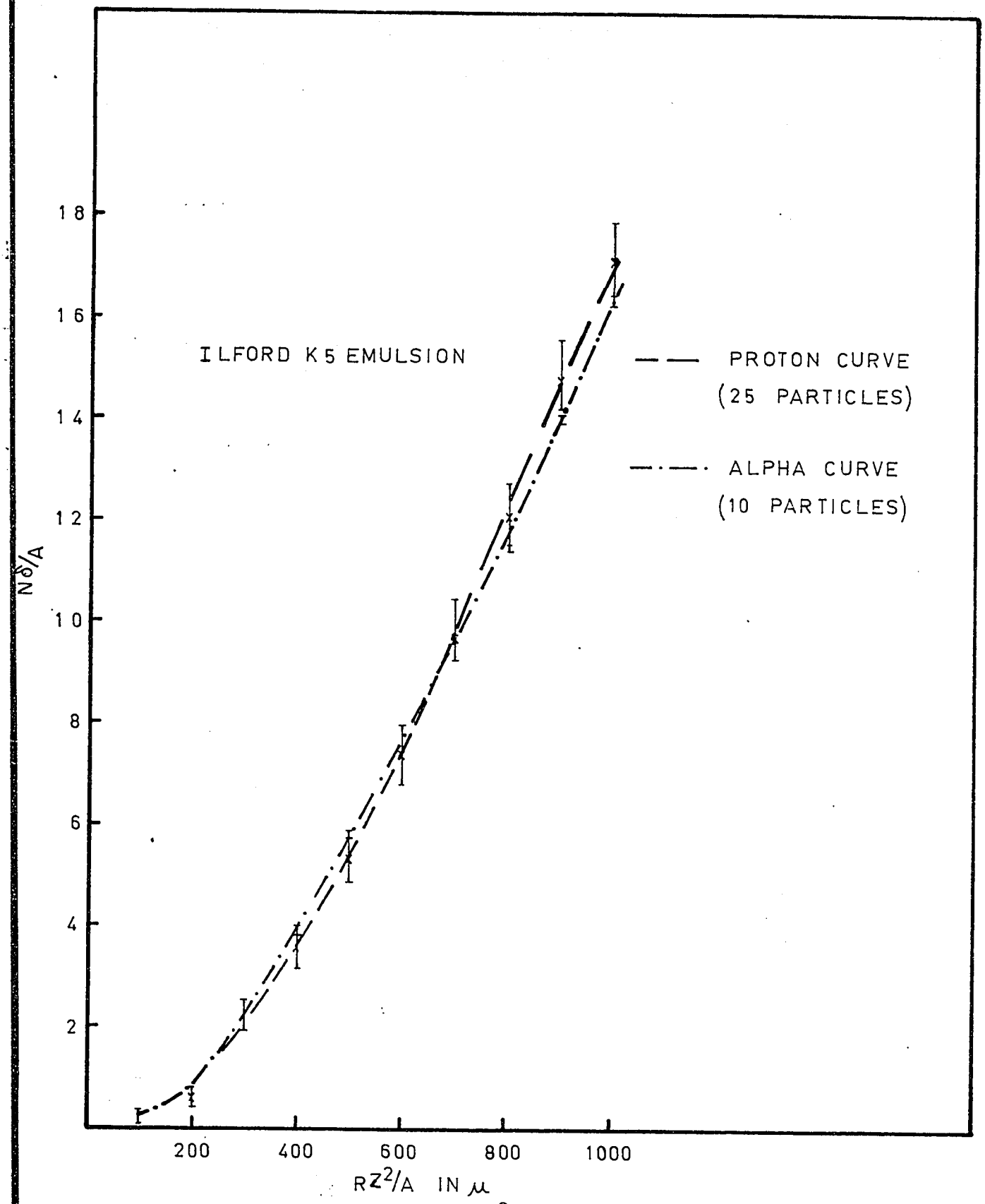

FIG. 5 PLOT OF Nδ/A VS RZ^2/A FOR α PARTICLES AND PROTONS.

Experimental integral curves for Ilford L-4, K-5 and G-5 are shown in Figure 4.

Figure 5 shows integral curves obtained by measurements on protons and α particles. This plot shows that the N/A vs $R\frac{Z^2}{A}$ plot is truly a universal curve, because the results for the proton and alpha particle curves agree within the limit of probable error in the proton calibration curve.

It is observed that the curves of n/A vs RZ^2/A obtained for the K5 and L4 emulsions differ only slightly, whereas the curves for the G5 emulsion is considerably displaced towards higher values of N/A. This is probably due to two causes:
(1) the developed grains in G5 emulsion are larger than those in the K5 and L4 emulsions (see Fig. 1);
and (2) the G5 emulsion is more strongly developed than the other two emulsions used.

These combined effects would, therefore, make it possible to count, in the G5 emulsion, slightly less energetic delta-rays than can be detected in the K5 and L4 emulsions, thus increasing the total number of delta-rays observed, with a resultant shift of the ratio N/A toward higher values.

(b) Track Width.

The width of a track formed by a heavily ionizing particle in nuclear emulsion is determined by the number of low-energy δ-rays produced at each point along the trajectory of the particle. As shown in the previous section, as the particle slows down, the linear density of the δ-rays of energy E_o increases, reaching a maximum value when $\beta^2 = E_o/m_o c^2$, and then falls rapidly to zero. The cut-off occurs at increasingly large velocities as the energy of the δ-rays increases. Hence, as the particle reaches the end of its range, the number of δ-rays produced will decrease rapidly as an increasing number of the higher energy δ-rays are cut off. We should, therefore, expect to observe a corresponding variation in the track width - an increase in width as the number of low-energy δ-rays increases, followed by a tapering of the track towards the end of the range. This effect becomes more pronounced as the charge, Z, of the ionizing particle increases, since the number of δ-rays produced varies as Z^2. Hence, as Z increases, we should expect to observe:

(1) an increase in the maximum thickness of the core;
and (2) a rapid decrease towards the end of the range of the thickness of the core.

The tapering at the extreme end of the range will also be enhanced by the effect of capture of electrons, producing a continuous decrease in the charge of the particle.

For singly charged particles the number of delta-rays produced is insufficient to produce a measurable variation in the track width. However, track width measurements are useful for the identification of light fragments.

Measurements of the variation of track width with residual range were made in Ilford L4, K5 and G5 emulsions and the results are shown in Figure 6. The tracks were previously identified from delta ray-range measurements.

These curves show that tracks due to particles of charge Z = 2 and Z = 3 can be separated by track-width measurements. Since we are not interested in identifying heavier fragments, no attempt was made to obtain curves for particles of higher Z.

In the L4 emulsion it was also possible to separate protons from α-particles by track-width measurements, but this separation could not be made in the K5 and G5 emulsions. This could be explained by the fact that in the L4 emulsion, the grains are smaller and of more uniform size than in the other two emulsions used. The larger statistical fluctuations in the grain size in the K5 and G5 emulsions make it more difficult to detect a small variation in grain size due to the ionization produced by the particle.

Track-width measurements are not reliable for the identification of tracks making large angles of dip with the emulsion. After processing the emulsion thickness is only about 2/5 of the original thickness (owing to the removal of undeveloped silver bromide during fixation). This shrinkage produces a

compression of the track, which results in an increase in track width for angles of dip greater than 30° in unprocessed emulsion.

(c) Gap Counts.

The number of developed grains per unit length of a track is a measure of the primary ionization produced by the particle. For particles near the end of their range (and for energetic particles of charge greater than 3), the grain density becomes too large to distinguish individual grains. In this case, groups of grains or "blobs" may be used as a measure of the ionization. A study of the variation of blob density, or the corresponding gap density, along a track, is a useful means of identifying particles of low Z.

The gap counts must be made under high magnification (100 x oil objective, 10 x eyepieces) and only those gaps which are clearly visible are counted. For angles of dip greater than 30° (unprocessed emulsion), gap count measurements are not reliable, owing to the shrinkage of the emulsion.

It was found that the method of gap counting was not possible in the L4 emulsion owing to the very small number of gaps observed. The results of gap count measurements in the G5 and K5 emulsions are shown in Figure 7, in which the integral gap density is plotted as a function of the residual range. Protons, α particles and particles of charge Z = 3 (or greater)

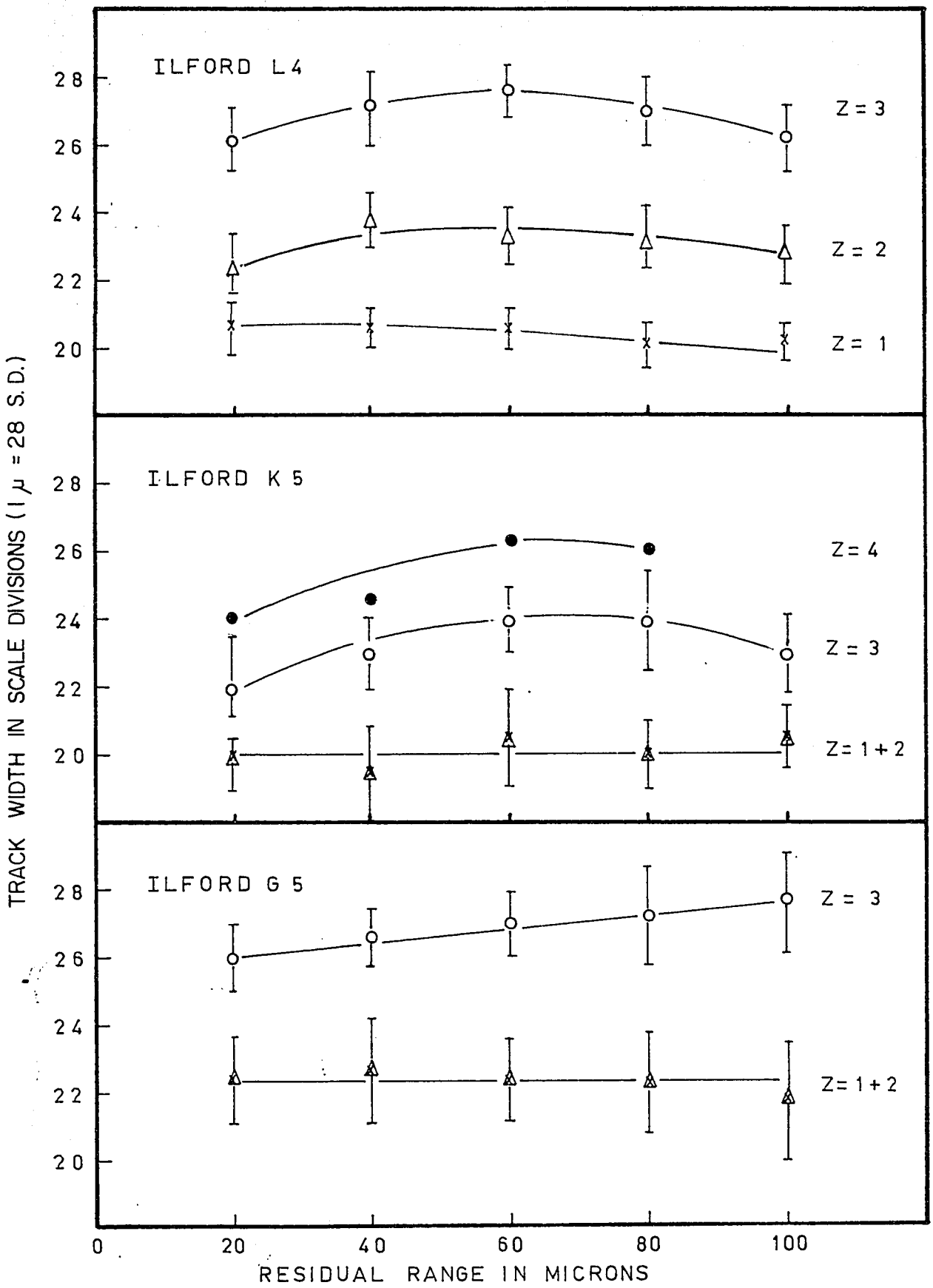

FIG. 6 TRACK WIDTH MEASUREMENTS IN L4, K5, G5, EMULSIONS.
(ERROR SHOWN IS STANDARD DEVIATION)

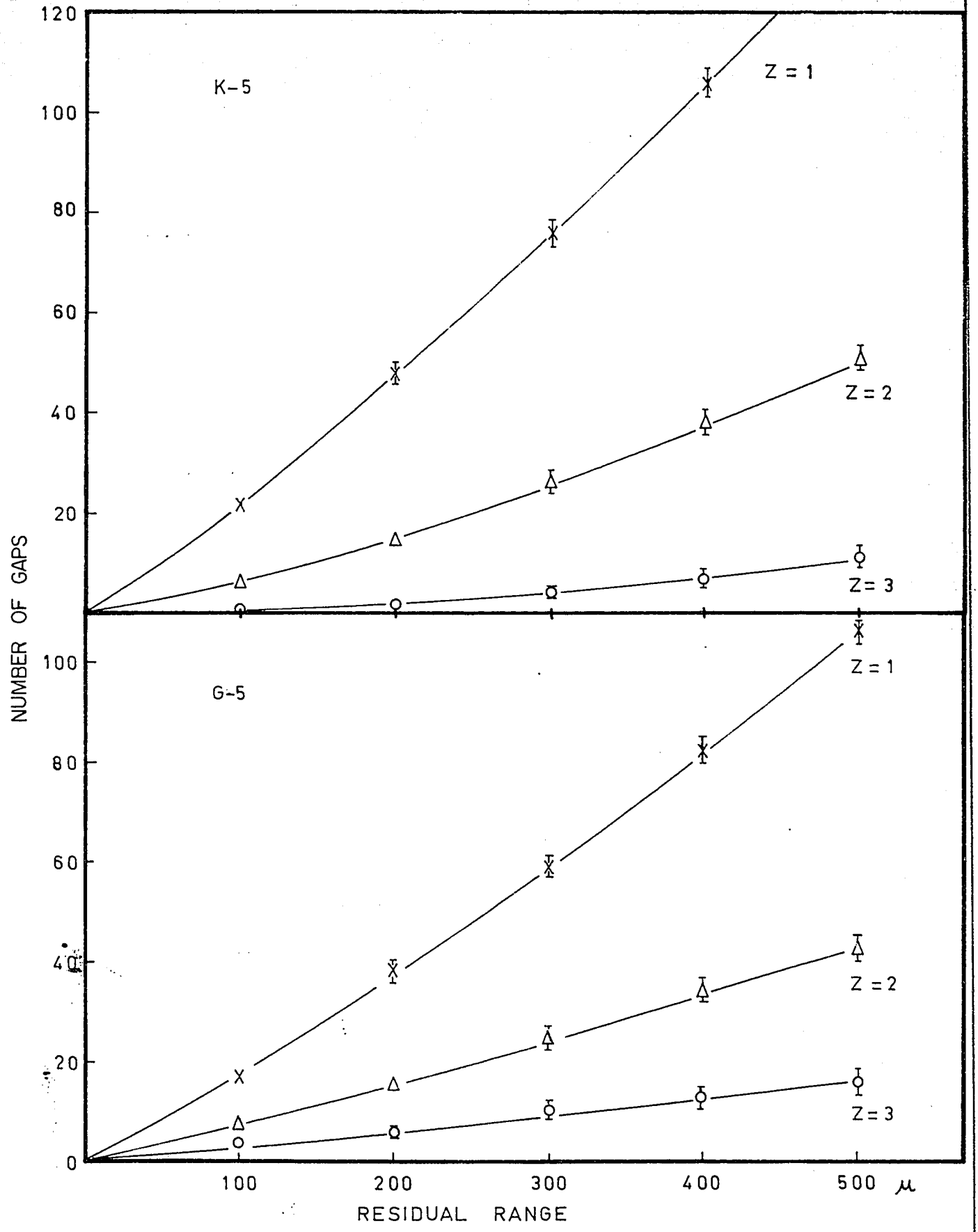

FIG. 7 INTEGRAL GAP COUNT CURVES FOR PARTICLES OF CHARGE Z=1,2,3.

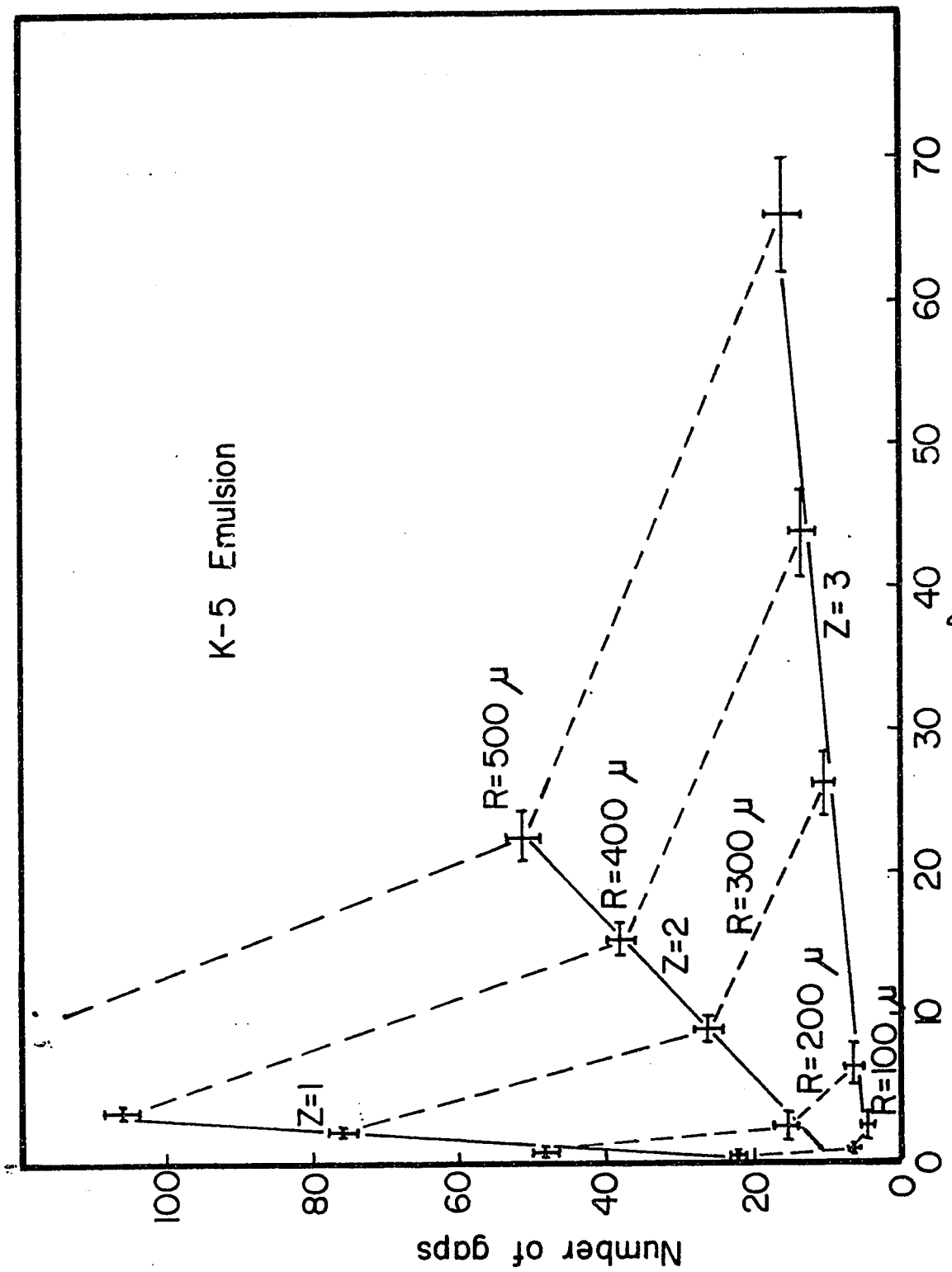

Fig. 8 The total number of gaps as a function of the total number of δ rays for successive range intervals of 100 μ

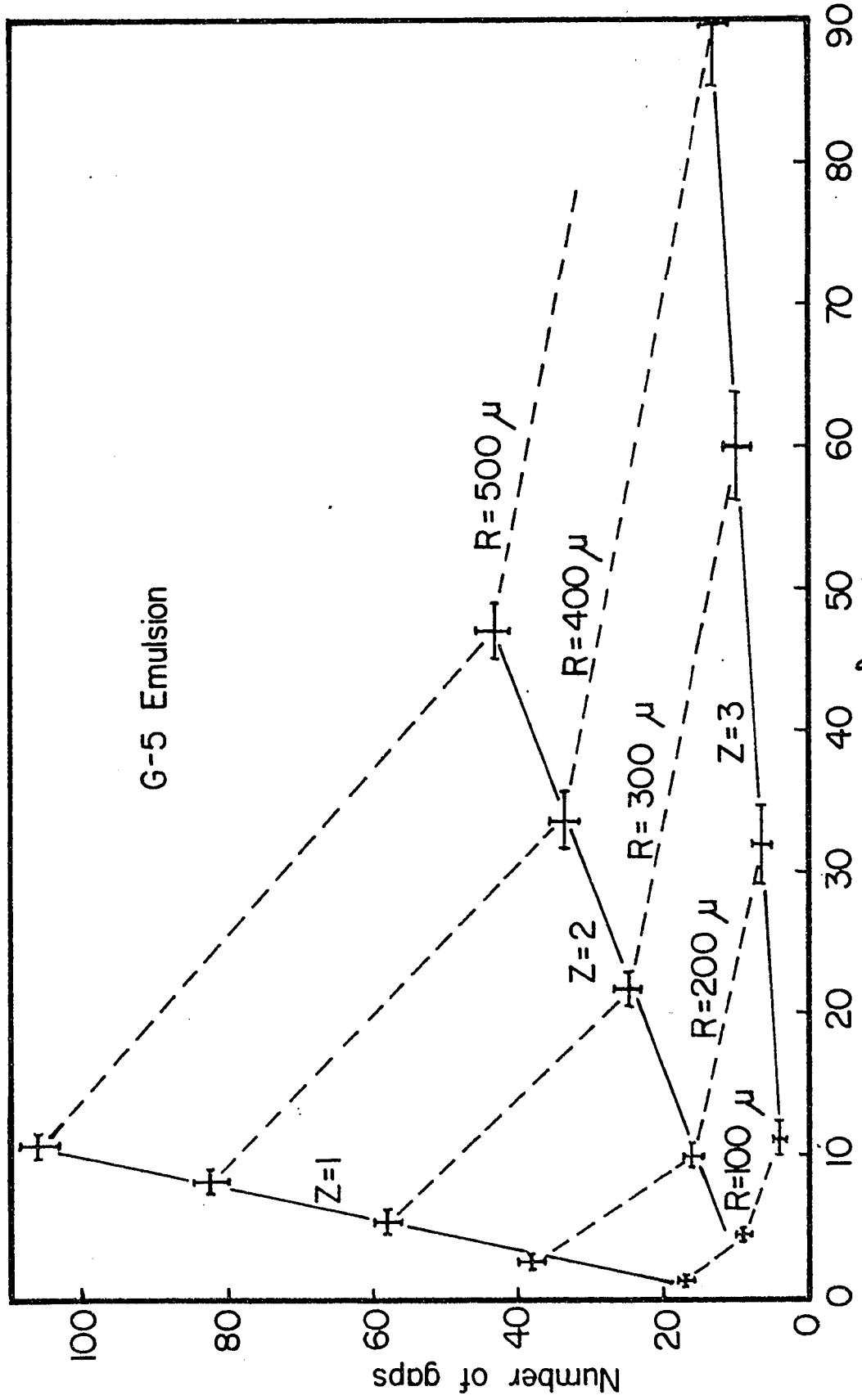

Fig. 9 The total number of gaps as a function of the total number of δ rays for successive intervals of 100 μ along tracks of particles of Z = 1, 2 and 3.

are well separated in both types of emulsion.

Figures 8 and 9 show a plot of the total number of gaps as a function of the total number of delta rays for successive range intervals of 100 μ. In both G-5 and K-5 emulsions, particles of charge Z = 1, 2 and 3 are easily separated by this procedure.

VI. Summary of Results.

For the identification of protons and α particles, two of the methods studied can be used for all three types of emulsion (L4, K5 and G5). These are:
(1) range-scattering measurements (useful only for long tracks); and (2) delta-ray measurements.

For the K5 and G5 emulsions, the method of gap-counting is also applicable.

For the L4 emulsion, track-width measurements may be used.

The last two types of measurements are easy to carry out and provide a rapid means of identification of particles of charge $Z \leq 3$. They are particularly useful for the study of very flat tracks. In the case of steeper tracks, the delta-ray measurements are most reliable, as the number of delta-rays is not affected by the shrinkage of the emulsion.

PART II.

Analysis of the Low-Energy Particles from Proton Interactions with Silver and Bromine Nuclei at 6 BeV and 27 BeV.

I. Evaporation theory.

(a) Theory of the Evaporation Process.

The interaction of a high energy particle with a complex nucleus results in a cascade of fast nucleons and mesons. Following the cascade ($t \sim 10^{-22}$ sec), the residual nucleus is left in a highly excited state (up to several hundred MeV). Assuming that the excitation energy is smaller than the total binding energy of the residual nucleons, one can then assume that the excitation energy is released by successive evaporations of particles (n, p, d, t, α, and fragments) from an approximate thermodynamic equilibrium state. (The evaporation may, in some cases, be accompanied by the fission of the excited nucleus).

The evaporation process has been treated theoretically by Weisskopf (1937). Later modifications of Weisskopf's theory were introduced by Le Couteur, Fujimoto and Yamaguchi[29], and Tomonaga[30]. These theories assume that the nucleons in the struck nucleus constitute a Fermi gas of free particles confined within the nuclear volume, W, and acted on by a force which can be represented by an average potential field. The nucleons occupy individual quantum states in the field and at any nuclear temperature, T, the distribution is given by the Fermi distribution. Le Couteur takes into account the expansion of

the nucleus with temperature as well as the neutron excess.

It is found that the number of particles N(E) of mass M and energy E escaping per second from a nucleus at a temperature T may be written in the form:

$$N(E)dE = \frac{\alpha NM}{2W}\{\exp - (\frac{B + V'}{T})\}\{(E - V')\exp - (\frac{E - V'}{T})\}dE, \qquad (1)$$

for $E > V'$ [for $E < V'$, $N(E)dE = 0$],

where N = total number of particles of mass M in the nuclear volume, W,

V' = effective height of the potential barrier,

B = binding energy of the particle,

and α is an appropriate constant.

Equation (1) can also be expressed in the simpler form

$$N(E)dE = k\,\frac{E-V'}{T^2}\,\exp^{-(\frac{E-V'}{T})}\,dE \qquad (2)$$

where k is an appropriate constant.

The maximum in the energy spectrum should occur at a value of E equal to $(V' + T)$, the sum of the effective mean values of the temperature and barrier height. The average energy of the singly charged particles will be equal to $(V' + 2T)$, so that observations of the mean energy and the position of the maximum in the spectrum allow an estimate of T.

The initial nuclear temperature T is related to the excitation energy U by the expression

$$U(\text{MeV}) = \frac{AT^2}{10} \qquad (3)$$

Having estimated T, this expression provides an estimate of U. This expression is in satisfactory agreement with measurements on the evaporation spectra of heavy nuclei.

(b) Points of Comparison of Theory with Experiment.

The applicability of the evaporation theory to the process of emission of the low-energy particles can be tested in three ways:-

(i) Angular distribution.

Due to the statistical nature of the evaporation process, the angular distribution of the evaporated particles should be isotropic in the centre of mass system.

(ii) Energy spectrum of the particles.

Evaporation theory predicts the shape of the energy distribution, in terms of the parameters T and V'. The position of the maximum in the energy spectrum and the average energy of the particles permits a determination of the values of the effective temperature and barrier height which give the best fit to the experimental results.

(iii) Emission Ratios.

Theory predicts the probabilities of emission of different types of particles. Le Couteur shows that for stars with more than seven black tracks (corresponding to interactions with heavy nuclei), the theoretical emission ratio of doubly

charged particles to the total number of particles (n_α/N) decreases with increasing star size. Since the charge of a particle is more easily determined than its energy, the observed emission ratio provides a convenient point of comparison with theory.

II. Experimental Methods and Results.

(a) Selection of Events.

The K5 and L4 emulsions irradiated with 6 BeV and 27 BeV protons, respectively, were area scanned for large stars. Stars with less than eight black tracks may be due to interactions with the light nuclei (C,N,O) in the emulsion or may be due to low energy interactions with the heavy nuclei (Ag,Br). Since it is impossible to distinguish between these two possibilities, these stars were not considered.

The results were obtained from a study of 96 stars, 52 at a proton energy of 6 BeV and 44 at a proton energy of 27 BeV. Figure 10 shows histograms of the frequency of stars as a function of the number of black tracks in the two plates studied. For the 44 stars used to study the 27 BeV interactions, the number of black prongs per star shows a fairly uniform distribution around a mean value of 13.9. The distribution for the 52 stars studied at an energy of 6 BeV appears to be somewhat different, the mean number of black prongs per star in this case being 12.7. However, the difference between the two

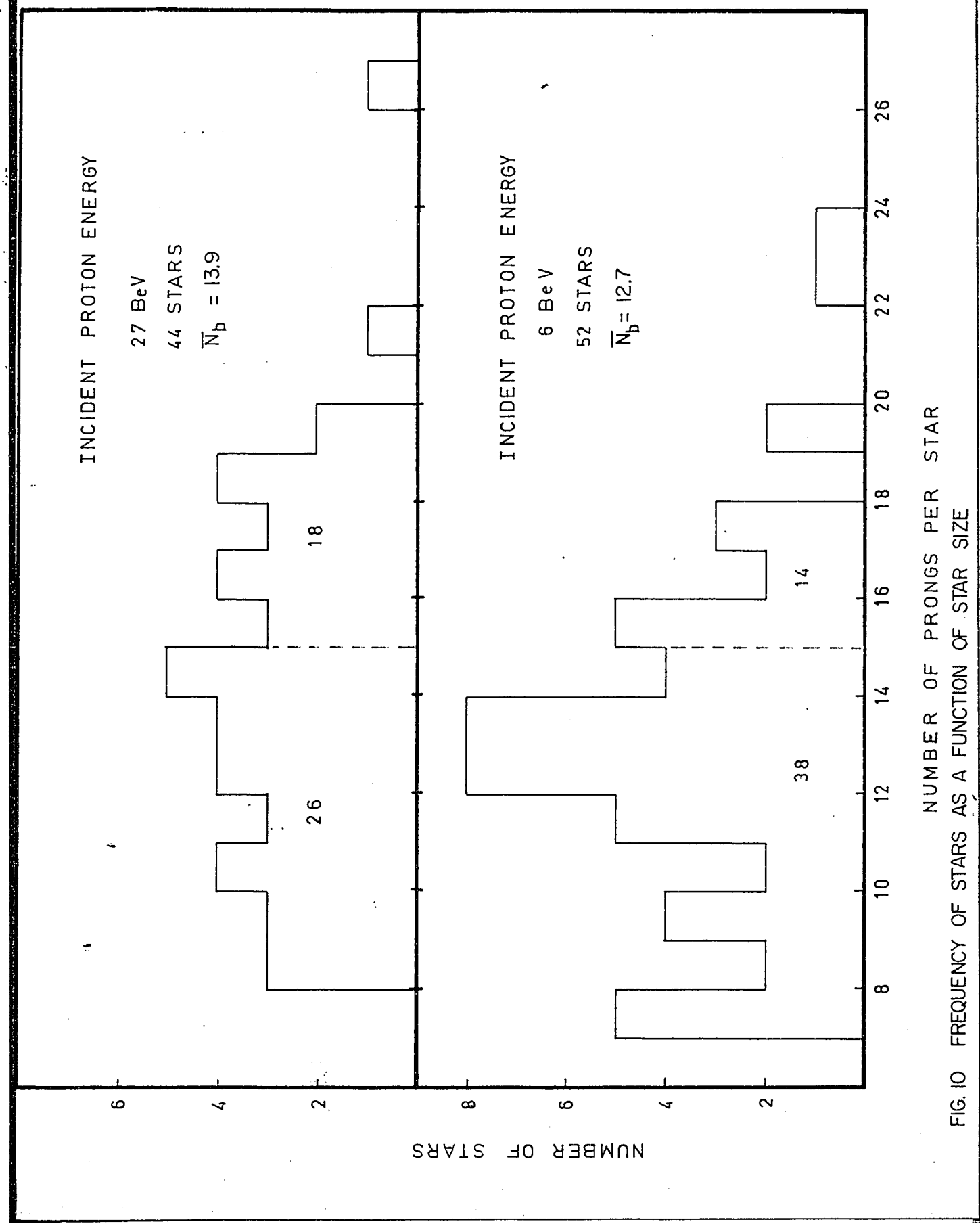

FIG. 10 FREQUENCY OF STARS AS A FUNCTION OF STAR SIZE

distributions is probably due only to the statistical fluctuations resulting from the small number of stars studied at each energy, since the method of scanning used should not have introduced a bias in the selection of events.

The protons and α particles among the black tracks were identified by the techniques described in Part I. Since the identification techniques are not reliable for steep tracks, the measurements were restricted to tracks for which the angle of dip in the unprocessed emulsion did not exceed 30°.

(b) Angular Distribution.

1. Experimental Determination.

The angular distribution of the identified α particles was determined for the interactions at 6 BeV and 27 BeV. The angle of emission, Θ, between the α particle and the incident proton is determined by the relation

$$\cos \Theta = \cos \alpha \cos \psi ,$$

where α is the projected angle in the plane of the emulsion and ψ is the angle of dip (see figure next page).

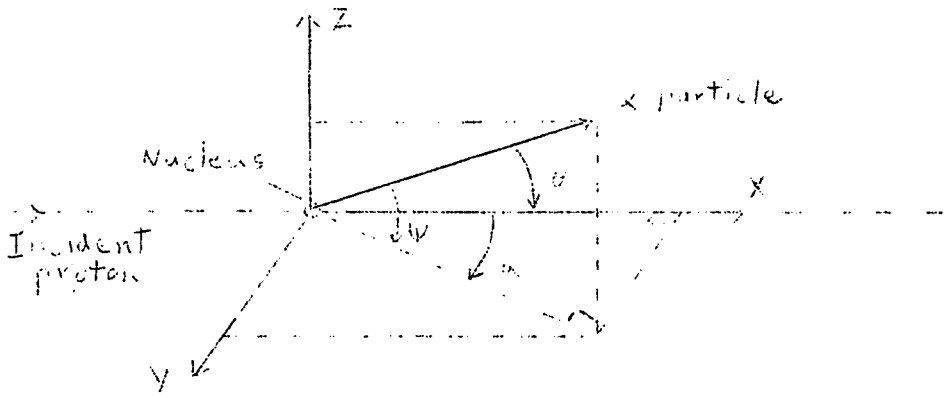

The value of α is measured by means of a goniometer eyepiece (or a protractor fitted to the ocular). The angle of dip ψ is determined from the horizontal and vertical projections, x and z, of the track, measured, respectively, with an eyepiece graticule and the fine focus depth calibration of the microscope. Hence, $\tan \psi = \frac{Sz}{x}$, where S is the shrinkage factor of the emulsion and corrects the vertical projections measured in processed emulsion to the corresponding values in the unprocessed emulsion. The shrinkage factor S is simply given by the ratio (thickness of unprocessed emulsion)/(thickness of processed emulsion), and usually has a value of about 2.5. The thickness of the processed emulsion is very sensitive to changes in relative humidity of the atmosphere, and to the swelling produced by the presence of immersion oil when using high-power objectives,

and so the shrinkage factor should be re-determined each day.

2. Correction of Measured Angular Distribution for Loss of Steep Tracks.

Since the experimental angular distribution is obtained only for α particles having angles of dip $\leq 30^{\circ}$, a geometrical correction factor has to be applied to correct for the loss of the steep tracks.

Figure 11 shows the limiting case when the angle of dip of the α particle is 30°. The base of the hemisphere represents the plane of the incident particle. Any track rising through the plane ABCD will not be measured. For a track making an angle θ with the direction of the incident particle,

$$r = R \sin \theta$$

and $\cos \varphi = h/r = h/R \sin \theta$, where φ is the azimuthal angle. Eliminating r,

$$\varphi = \cos^{-1} \left(\frac{h}{R \sin \theta}\right)$$

But for the limiting case where the angle of dip is 30°

$$h = R \sin 30^{\circ}$$

$$\varphi = \cos^{-1} \frac{\sin 30^{\circ}}{\sin \theta}$$

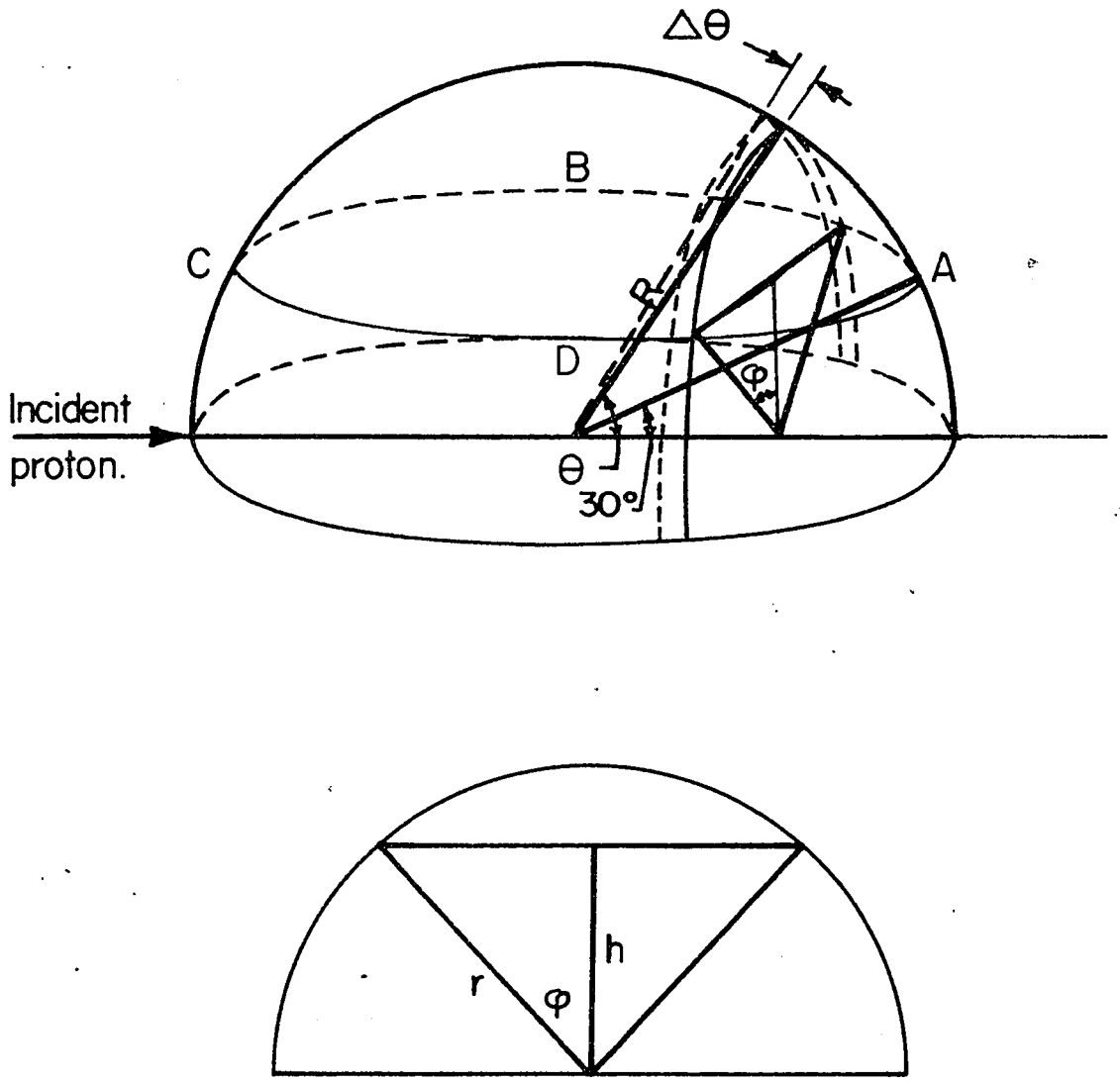

Fig. 11 Determination of correction factor for loss of steep tracks.

Now let θ increase by $\Delta\theta$. Then the tracks with angles of dip greater than 30° are contained within the portion of the annular ring of area ΔS cut-off by the plane ABCD. The fraction of the annular area cut-off is given by

$$f = \frac{4\varphi}{2\pi} = \frac{2}{\pi} \cos^{-1} \left(\frac{\sin 30^\circ}{\sin \theta}\right)$$

If θ increases from θ_1 to θ_2, we can write, to a first approximation,

$$f = \frac{2}{\pi} \cos^{-1} \left(\frac{1}{2 \sin\left(\frac{\theta_1 + \theta_2}{2}\right)} \right)$$

substituting $\sin 30^\circ = \frac{1}{2}$.

Hence, for any angular interval from θ_1 to θ_2, the fraction of tracks measured is

$$F = (1 - f) = 1 - \frac{2}{\pi} \cos^{-1} \left(\frac{1}{2 \sin \frac{\theta_1 + \theta_2}{2}} \right)$$

Table I shows the calculated values of F for intervals of θ corresponding to a variation in $\cos \theta$ of 0.1. For values of $\cos \theta \geq 0.866$ ($\theta < 30^\circ$), the correction factor 1/F is equal to 1. Since the correction is symmetrical about $\theta = 90^\circ$, the same correction factors apply to the particles emitted in the backward hemisphere.

Table I

Correction factor to be applied for the loss of steep tracks.

cos θ	F	1/F
1 → 0.9	1	1
0.9 → 0.8	0.82	1.2
0.8 → 0.7	0.55	1.8
0.7 → 0.6	0.46	2.2
0.6 → 0.5	0.41	2.4
0.5 → 0.4	0.38	2.6
0.4 → 0.3	0.36	2.8
0.3 → 0.2	0.35	2.9
0.2 → 0.1	0.34	2.9
0.1 → 0	0.33	3.0

3. Experimental Results.

The histograms (dotted lines) in Figures 12 and 13 show, respectively, the observed angular distributions of 118 α particles from the 6 BeV interactions and 101 α particles from the 27 BeV events. The distributions corrected for the effect of the loss of steep tracks are shown by the full lines in the figures.

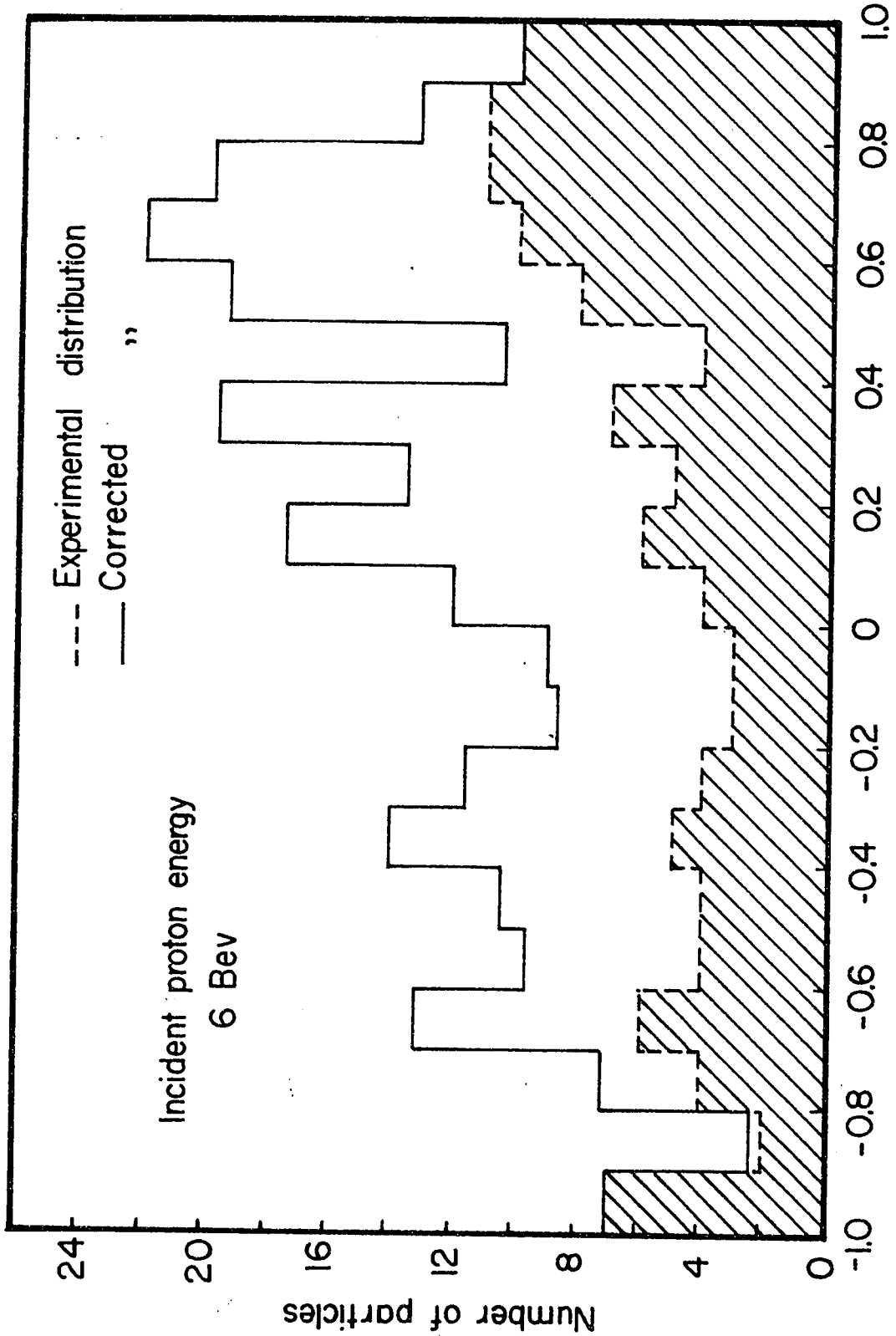

Fig. 12 Angular distribution of α particles emitted from Ag and Br nuclei.

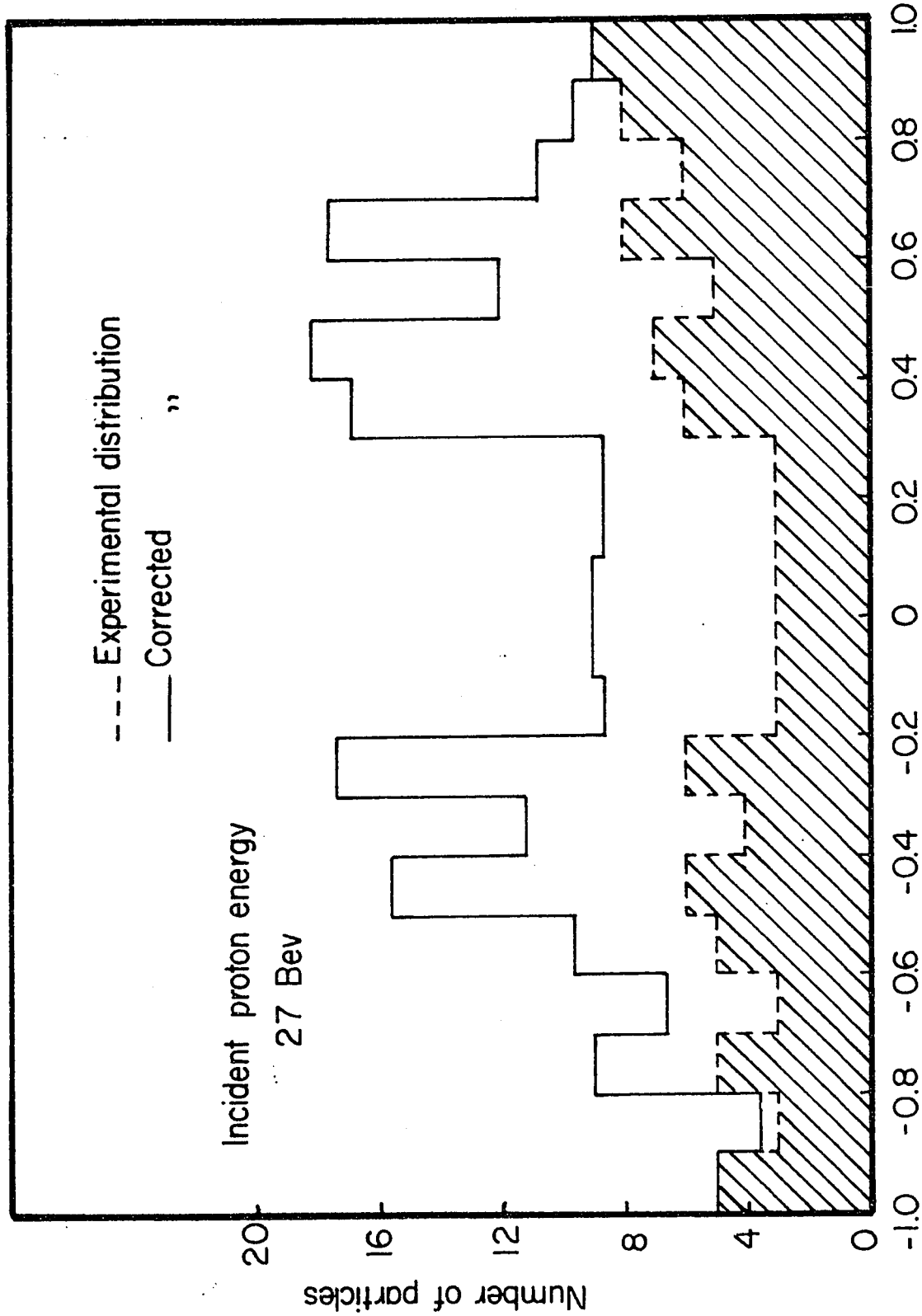

Fig. 13 Angular distribution of α particles emitted from Ag and Br nuclei.

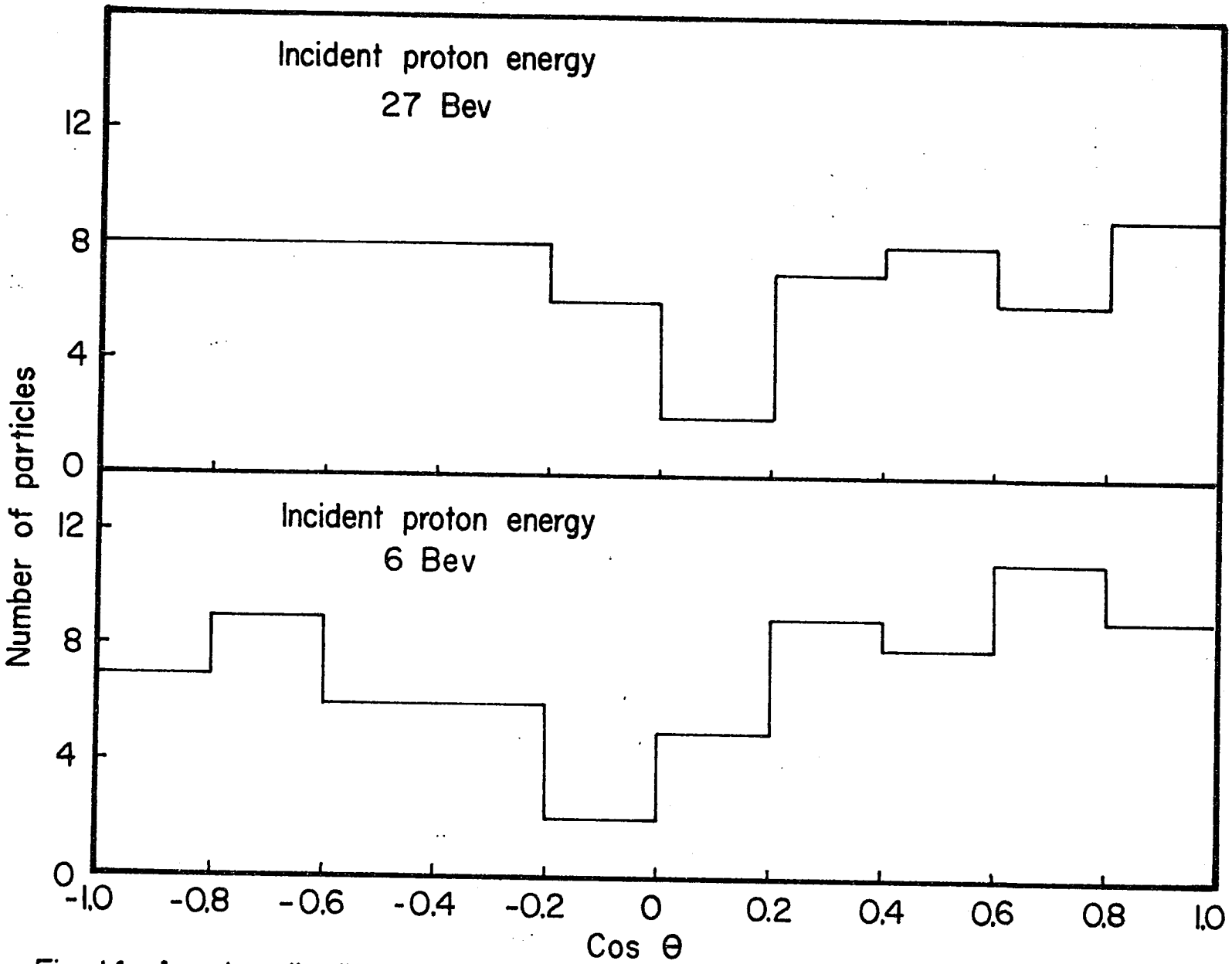

Fig. 14 Angular distribution of low energy α particles ($E_\alpha < 30$ Mev) emitted from Ag and Br nuclei.

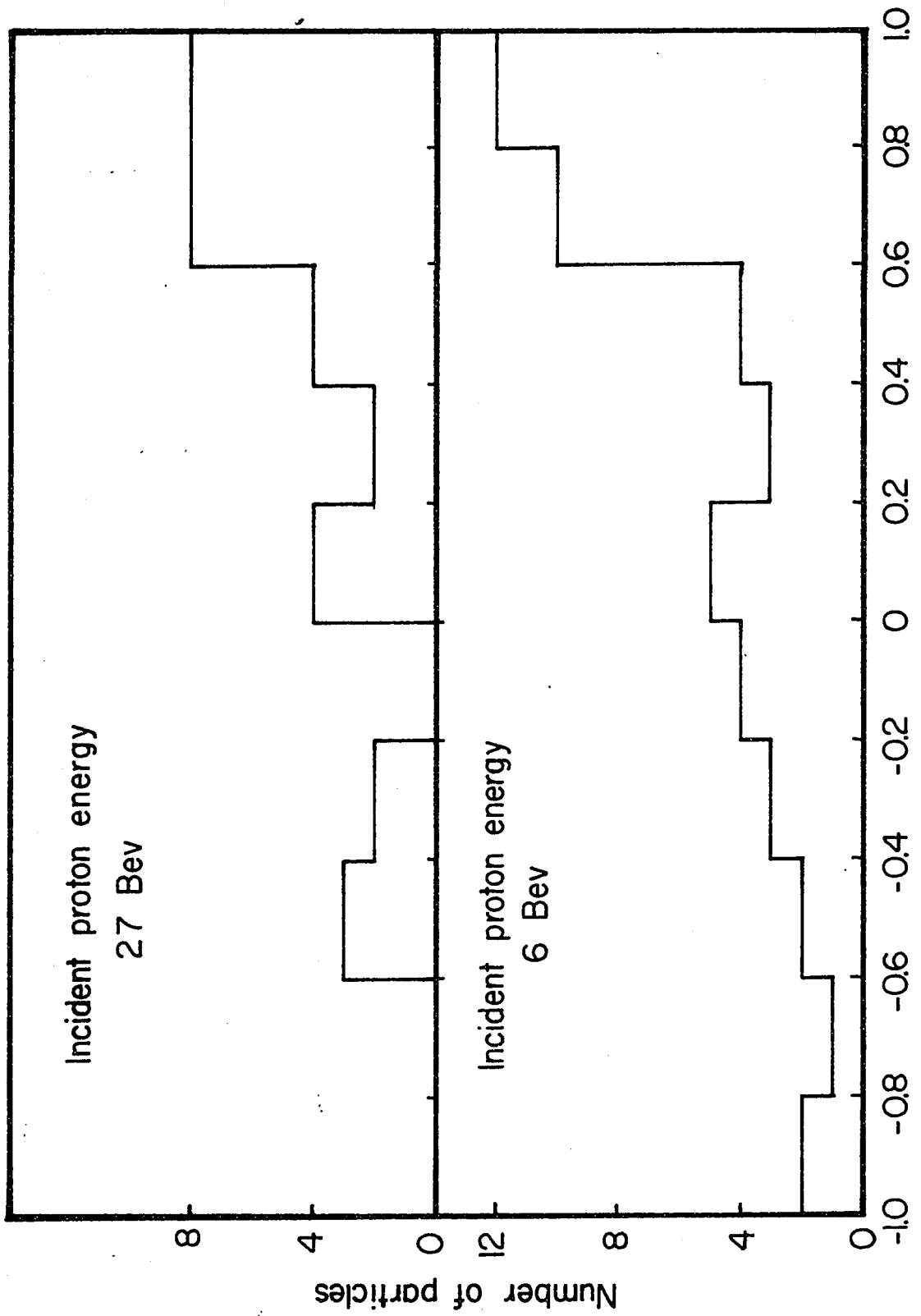

Fig. 15 Angular distribution of energetic α particles ($E_\alpha > 30$ Mev) emitted from Ag and Br nuclei.

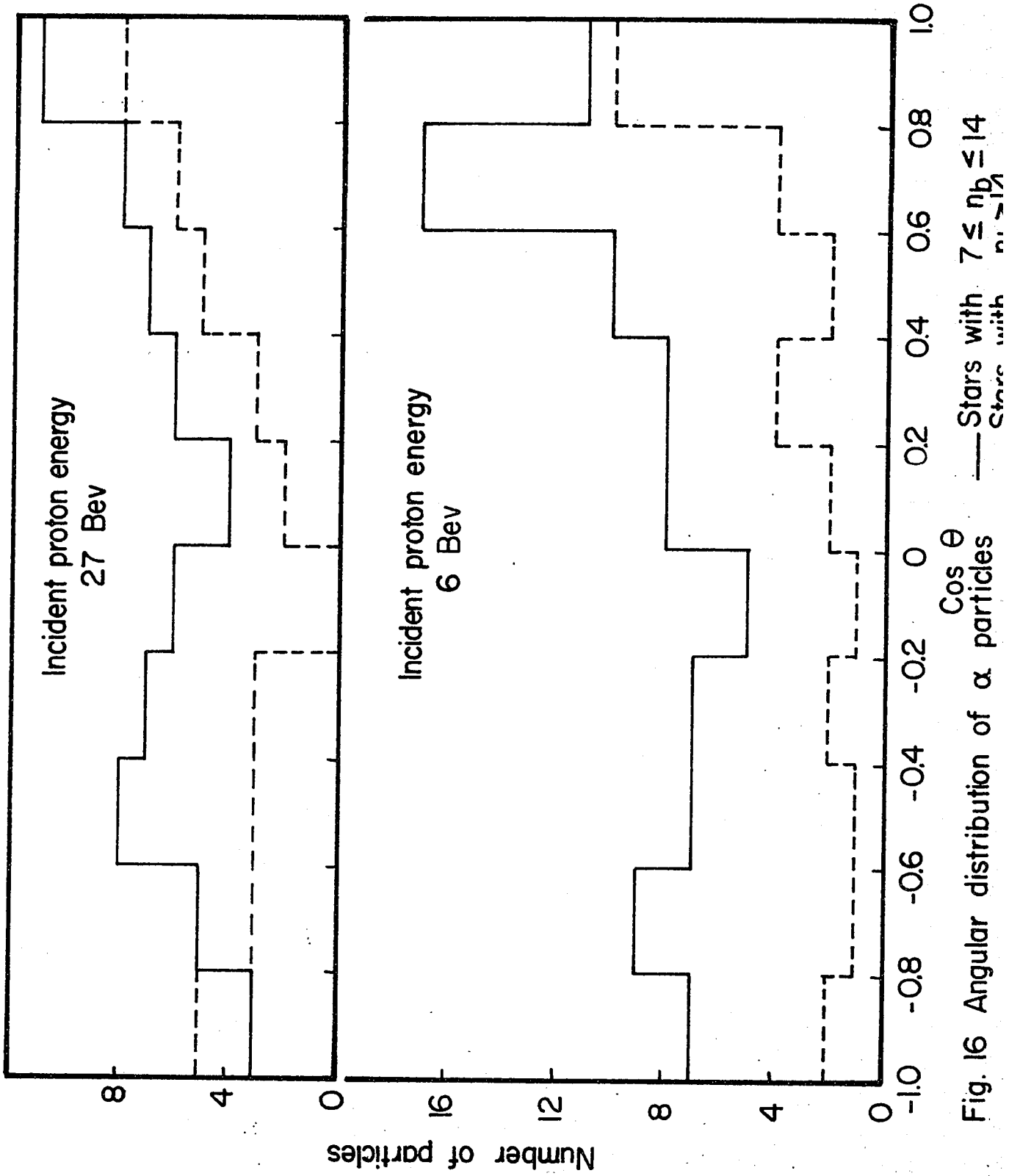

Fig. 16 Angular distribution of α particles

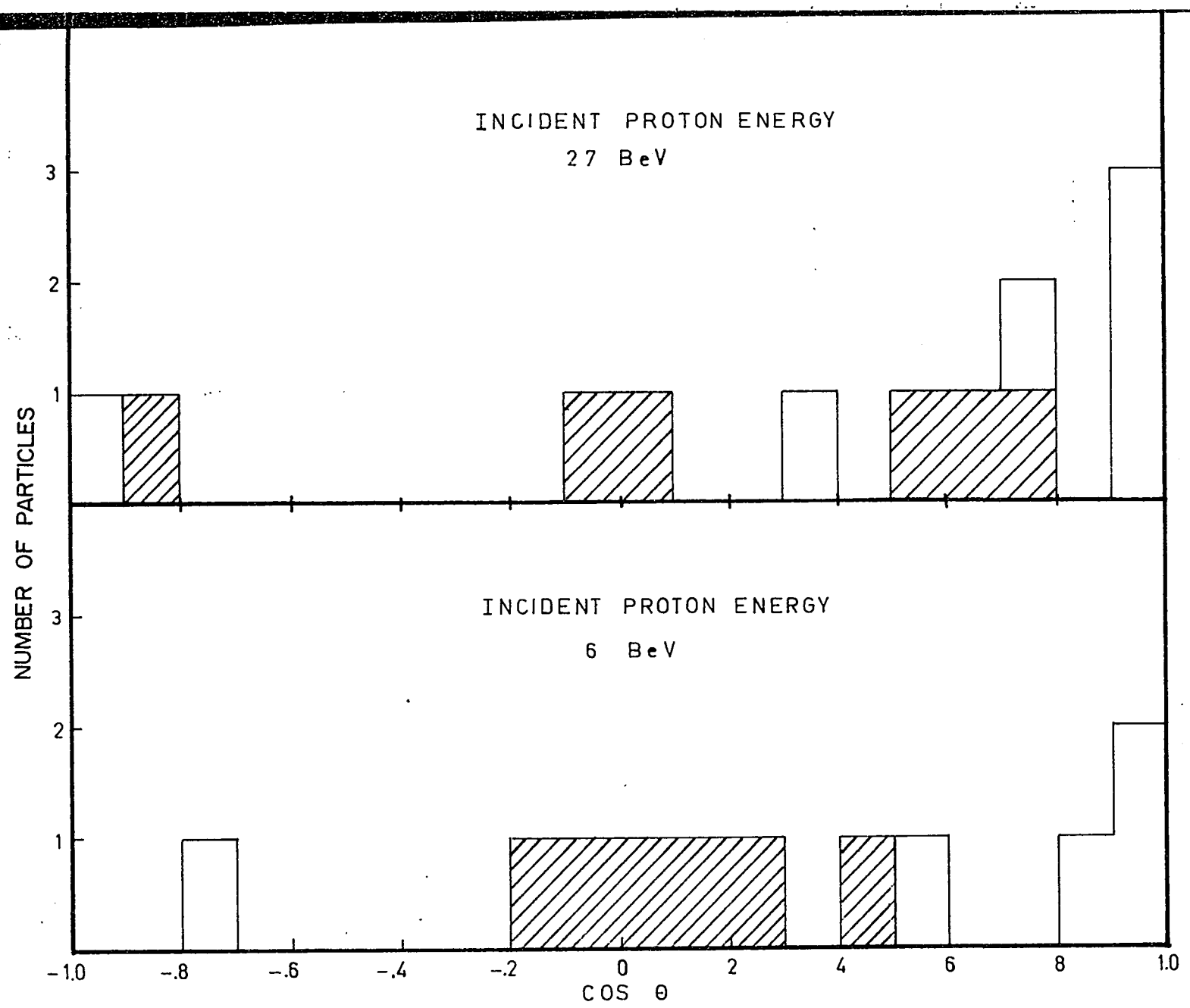

FIG.17 ANGULAR DISTRIBUTION OF LIGHT FRAGMENTS EMITTED FROM Ag + Br NUCLEI

▨ STEEP TRACKS.

In Figures 14 and 15 are shown the α particle angular distributions at 6 BeV and 27 BeV for two energy regions.

(a) α particles of energy < 30 MeV.

(b) α particles of energy > 30 MeV.

The two energy regions were defined in this manner because evaporation theory predicts that the probability of emission of α particles with an energy exceeding 30 MeV is small.

Since evaporation theory applies to stars with less than 15 black tracks, the α particles were divided into two groups:

a) α particles from stars with $n_b > 14$;

b) α particles from stars with $7 \leq n_b \leq 14$.

The angular distributions are compared in Figure 16.

The angular distribution of light fragments $Z \geq 3$ was also determined, and is shown in Figure 17. Approximately half of the tracks analysed were emitted at an angle of dip exceeding 30° (shaded area) but they were easily identified as fragments due to their extreme track width.

4. Comparison with Theory.

The two α particle angular distributions at 6 BeV and 27 BeV show that more particles are emitted in the forward hemisphere than in the backward hemisphere. This effect seems to be more important at 6 BeV than at 27 BeV. However, it is observed that the angular distributions for the α particles of

energy < 30 MeV are essentially isotropic, for the interactions at both 6 BeV and 27 BeV, in agreement with evaporation theory. The α particles of energy > 30 MeV are emitted predominantly in the forward direction. The forward/backward ratio is found to be 34:12 and 26:5 at 6 BeV and 27 BeV, respectively. The strong forward peaking observed at higher energies can explain the anisotropic distributions obtained for particles of all energies.

Figure 16 shows that the forward peaking is common to both the large and small stars, the effect being strongest in the large stars at an incident proton energy of 6 BeV.

We may, therefore, conclude that the angular distribution of the lower energy α particles (< 30 MeV) is consistent with evaporation theory. The higher energy α particles, however, cannot be explained in terms of a normal evaporation process from an equilibrium state of the excited nucleus. [A slight forward peaking of the angular distribution in the laboratory system could be attributed to the motion of the heavy excited nucleus. Baker and Katcoff[14] find that the mean velocity of the moving system, β, is .01 - .02, and for such a velocity the transformation from the laboratory system to the system of the centre-of-mass would reduce the forward to backward asymmetry, but would not eliminate it]. The predominantly forward emission of these particles indicates that they are associated with the initial cascade interaction of the incident proton; these α particles may be emitted as the result of secondary interactions

initiated by the recoiling nucleons produced in the initial collision.

It is interesting to note that, in spite of the poor statistics, the angular distribution of the light fragments indicates a preferential emission in the forward direction. Combining the distributions at 6 BeV and 27 BeV, the forward/backward ratio of light fragments is found to be 17:6, which is almost the same as the ratio found in the case of the energetic α particles (60:17). It is, therefore, possible that some of the fragments are emitted in the same type of process as the energetic α particles, the production occurring in the initial stages of the interaction.

(c) Energy Spectra.

The most accurate method of determining the energy of a particle is from a measurement of its range. This method obviously restricts the measurements to tracks ending in the emulsion and hence introduces a bias in favour of the lower-energy particles. However, since the present investigation is not concerned with the energetic shower particles, range-energy measurements provide a satisfactory method of determining the energy spectra of the evaporated particles.

1. Range-Energy Relation.

For protons of energy exceeding a few MeV, it has been shown experimentally[31,32] that the range-energy relation can be represented by an equation of the form

$$E_p = kR_p^r \qquad (1)$$

where E_p = proton energy in MeV,

R_p = proton residual range in mircons,

and k and r are constants which are determined experimentally.

More generally, for a particle of mass number M($M = \frac{m}{m_p}$, where m is the mass of the particle and m_p is the mass of the proton) and charge number Z, the range-energy relation is given by

$$E_M = kM\left(\frac{Z^2 R_M}{M}\right)^r$$

$$\text{or} \qquad E_M = kZ^{2r} M^{1-r} R_M^r \qquad (2)$$

The constants have been determined[31] for proton energies between 5 MeV and 50 MeV and are found to be:

$$k = 0.251 \; ; \; r = 0.581 \; .$$

For particles with low charge ($Z < 10$) the values of the energy deduced from equation (2), k and r having the values given above, are acceptable for ranges exceeding 0.1 cm. However, for shorter residual ranges the effect of capture and loss of electrons near the end of the range must be accounted for.

The effective charge of the particle is thus reduced and the simple relation expressed in equation (2) ceases to be valid. In the case of protons and α particles, capture and loss is confined to the extreme end of the range and the effect on the range-energy relation is small. It has been shown that for α particles the effect of capture and loss is to increase the ranges of the α particles, compared with those of protons of the same velocity, by a constant amount, approximately equal to 1.5 μ. This effect is, therefore, negligible except for very short tracks.

2. Experimental Determination of Range.

The range of a particle is determined experimentally from measurements of the projected range, x, in the plane of the emulsion and the vertical projection, z, of the track. Hence, the range R is given by

$$R = (x^2 + S^2z^2)^{1/2}$$

where S is the shrinkage factor of the emulsion.

The projected range is measured by means of a linear scale in the ocular; the vertical projection is determined from the difference in the readings on the fine focus depth calibration of the microscope when focussed on the first and last grains of the track.

For long tracks it is more convenient to use stage micrometers to determine the x and y components of the range in the plane of the emulsion. The range R is then given by the relation

$$R = (x^2 + y^2 + S^2 z^2)^{1/2}$$

The tracks of protons and α particles ending in the emulsion were selected from the particles previously identified from the study of the 52 stars produced by 6 BeV incident protons and the 44 stars resulting from the interactions at 27 BeV. From the measurements of the ranges of the particles, the energies were determined from the experimental range-energy relationship, using the tables prepared by Fay, Gottstein and Hain[28].

For those tracks not ending in the emulsion (observed to be 10 to 15% of all tracks for which the angle of dip is less than 30°), the range was estimated by comparing the gap density and the δ ray density, in the visible portion of the track, to other tracks, of the same charge, ending in the emulsion. From this approximate range an approximate energy was assigned to each track.

3. Experimental Results.

Figure 18 shows the proton energy spectra measured at 6 BeV and 27 BeV incident proton energies, the two spectra having approximately the same number of tracks. No significant difference is observed in the two spectra. The mean energy of

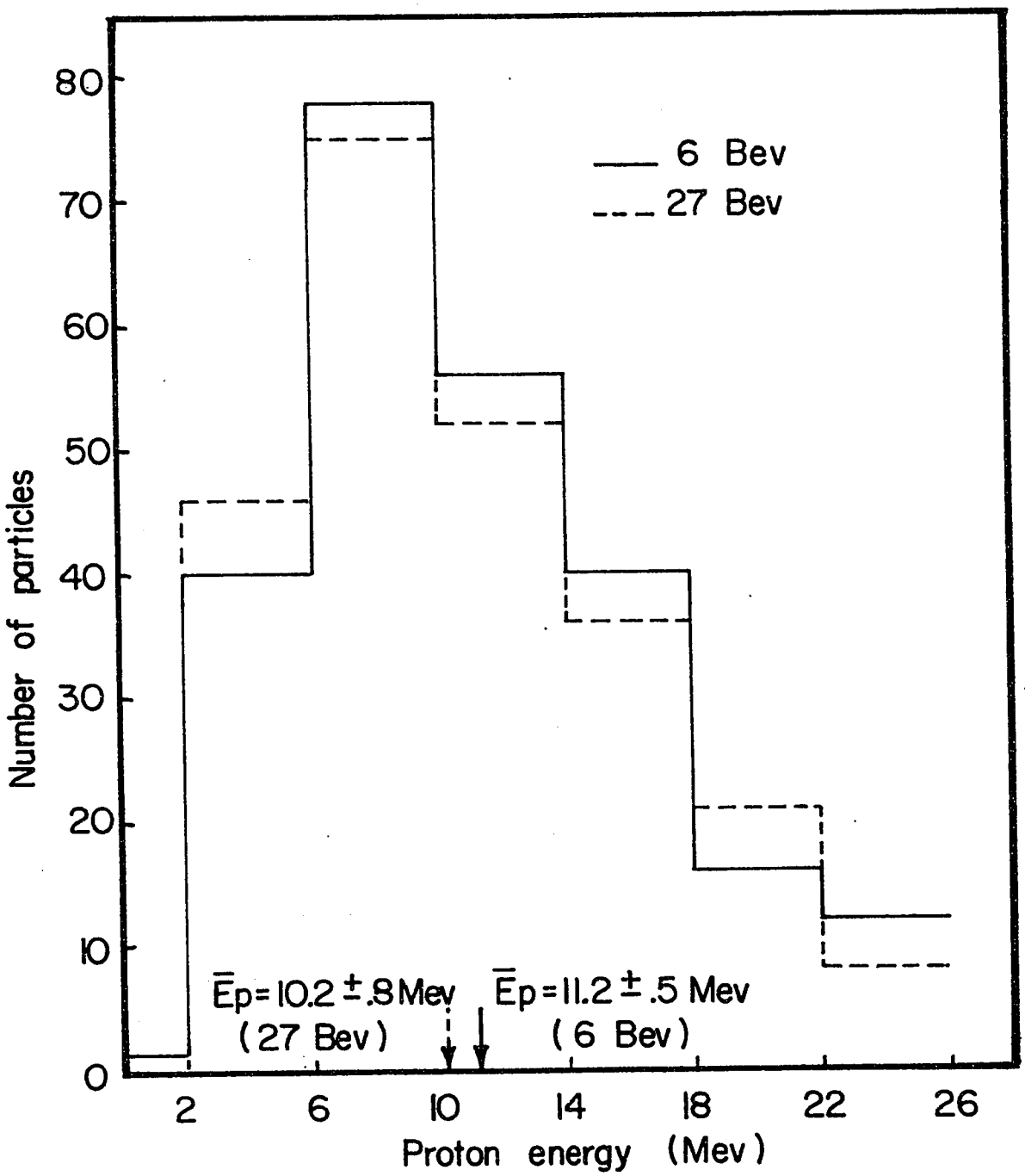

Fig. 18 Proton energy spectra.

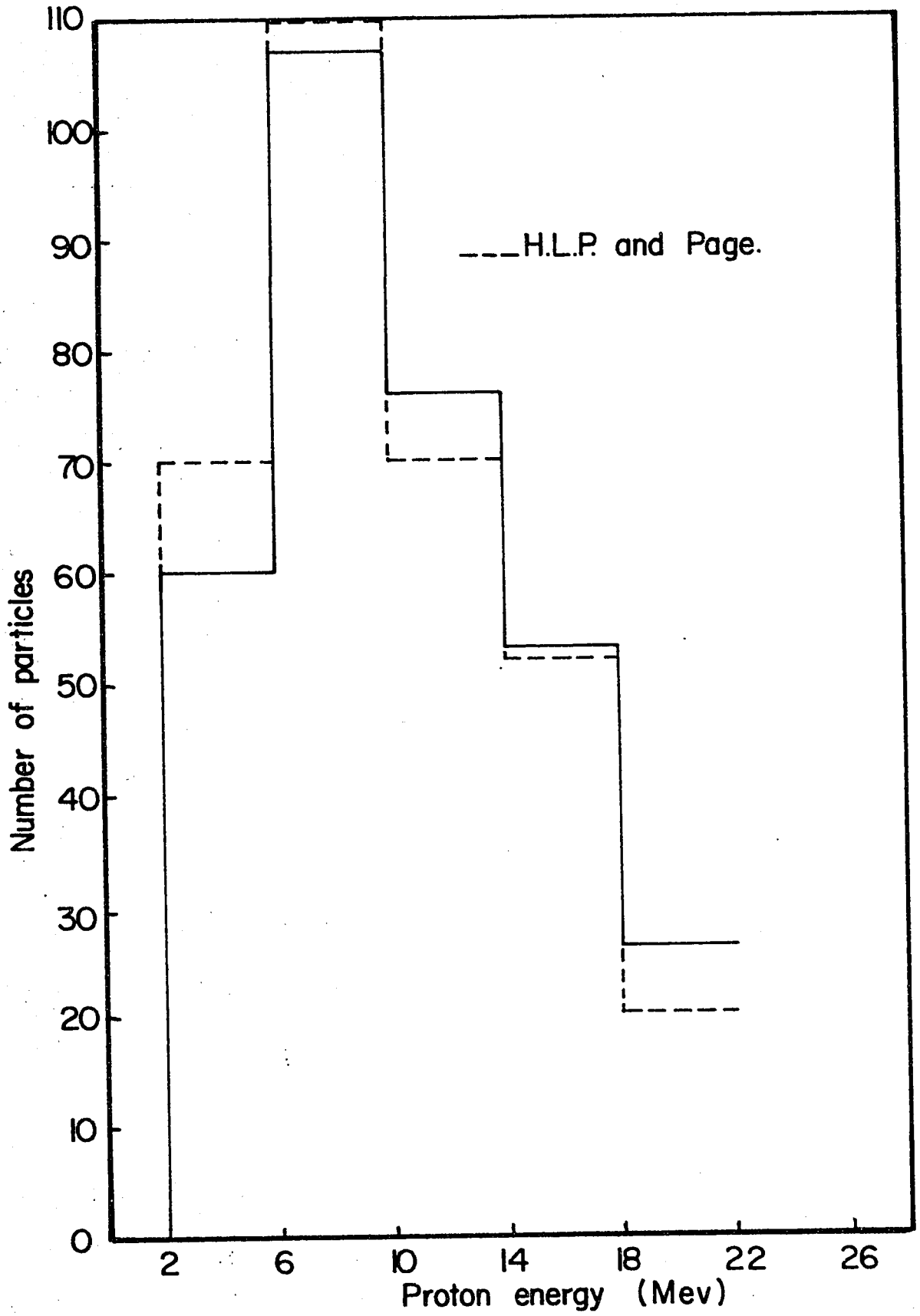

Fig. 19 Comparison of combined energy spectrum with experimental results of H.L.P. and Page.

the evaporated hydrogen nuclei (having an energy per nucleon less than 26 MeV) is found to be (11.2 ± 0.5) MeV for the 6 BeV interactions, and (10.2 ± 0.8) MeV for the interactions at 27 BeV.

In Figure 19, the two spectra are combined and compared to the experimental results of Harding, Lattimore and Perkins for stars produced at cosmic ray energies, and of Page for interactions with 660 MeV protons. The combined spectrum was normalised to the same number of tracks as the spectrum of H.L.P. and Page. The agreement is fairly good.

The energy spectra of the doubly charged particles are shown in Figure 20. The two spectra are similar, the only differences being a slight excess of high-energy particles in the spectrum at 6 BeV. According to evaporation theory, the energy distribution should drop off sharply for α particle energies greater than 30 MeV. Both the experimental spectra obtained show a long tail at the high-energy end.

Since the techniques used for the identification of particles are not applicable to tracks of range less than 30 μ, the majority of α particles with energy less than 8 MeV have been excluded. A similar study by J. Hébert and J. Hébert[32], made at 18 BeV, using less sensitive emulsion (K minus 1) shows that the number of α particles with energy between 0-8 MeV is approximately 60% of the number with energy between 8-16 MeV. Furthermore, the number of α particles with energy between 4-8 MeV is twice the number with energy between 0-4 MeV. These

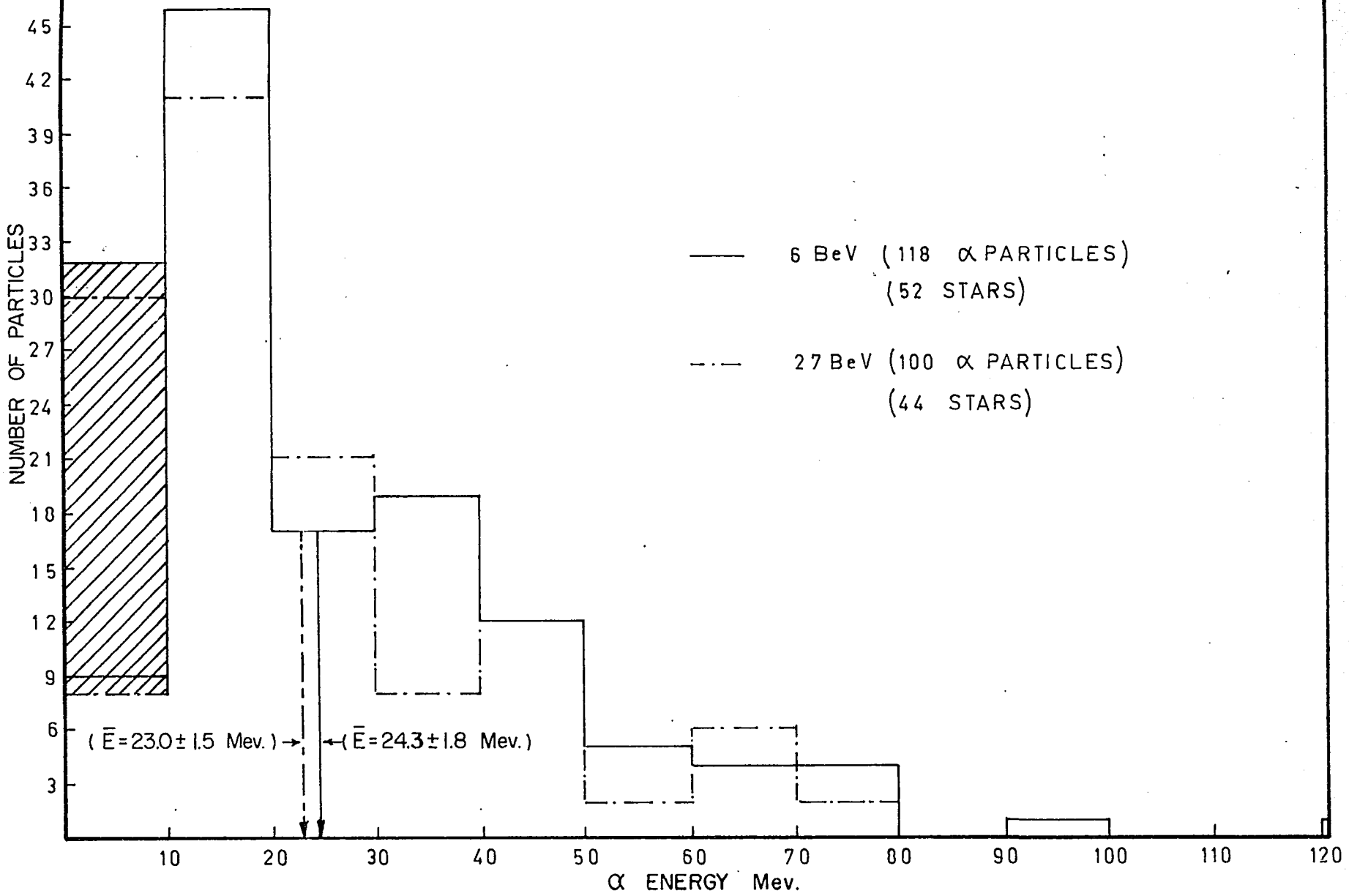

FIG. 20 ALPHA PARTICLE ENERGY SPECTRA (SHADED AREA REPRESENTS CORRECTION FOR LOSS OF LOW ENERGY PARTICLES)

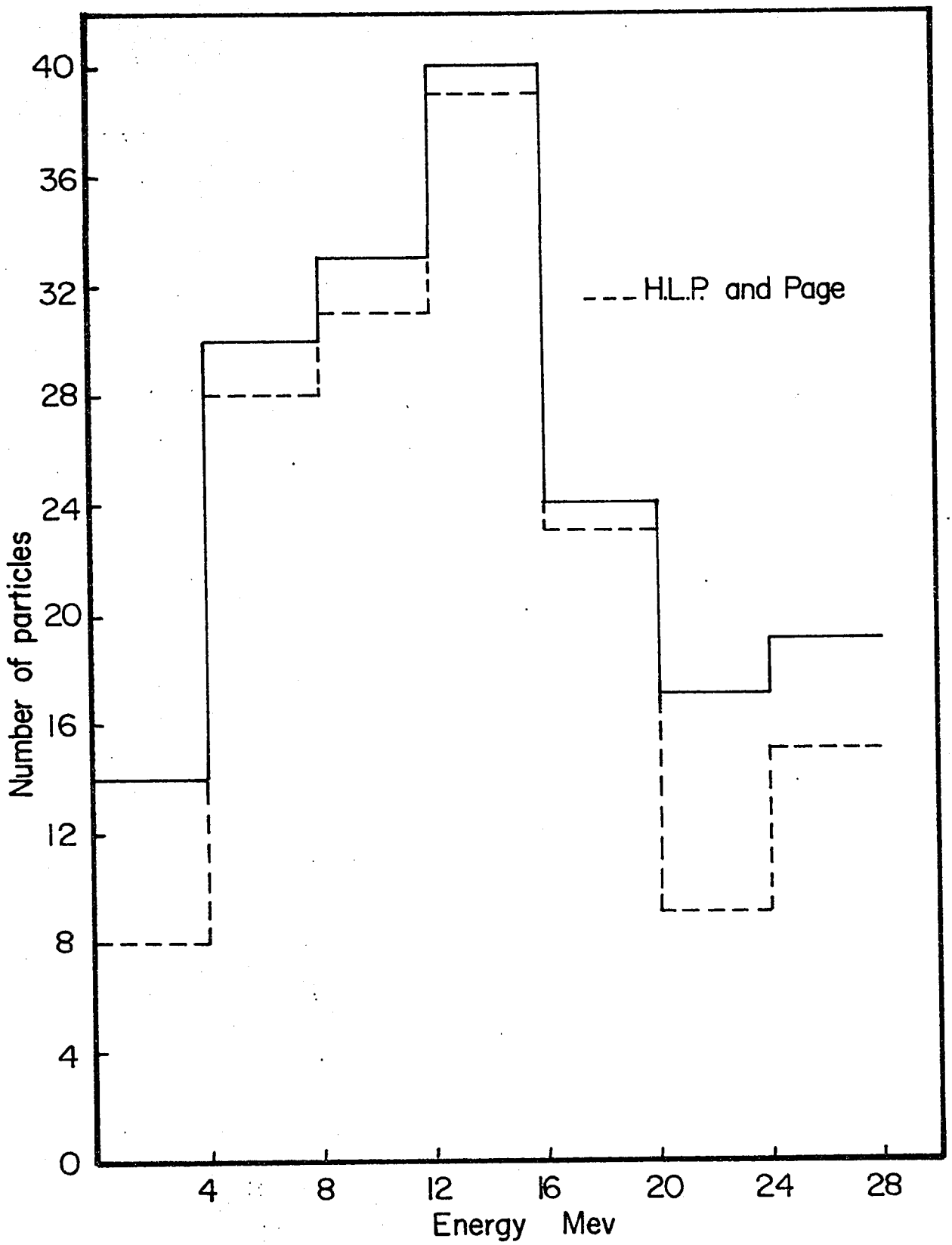

Fig. 21 Comparison of low energy α particle spectrum (E_α<30 Mev)

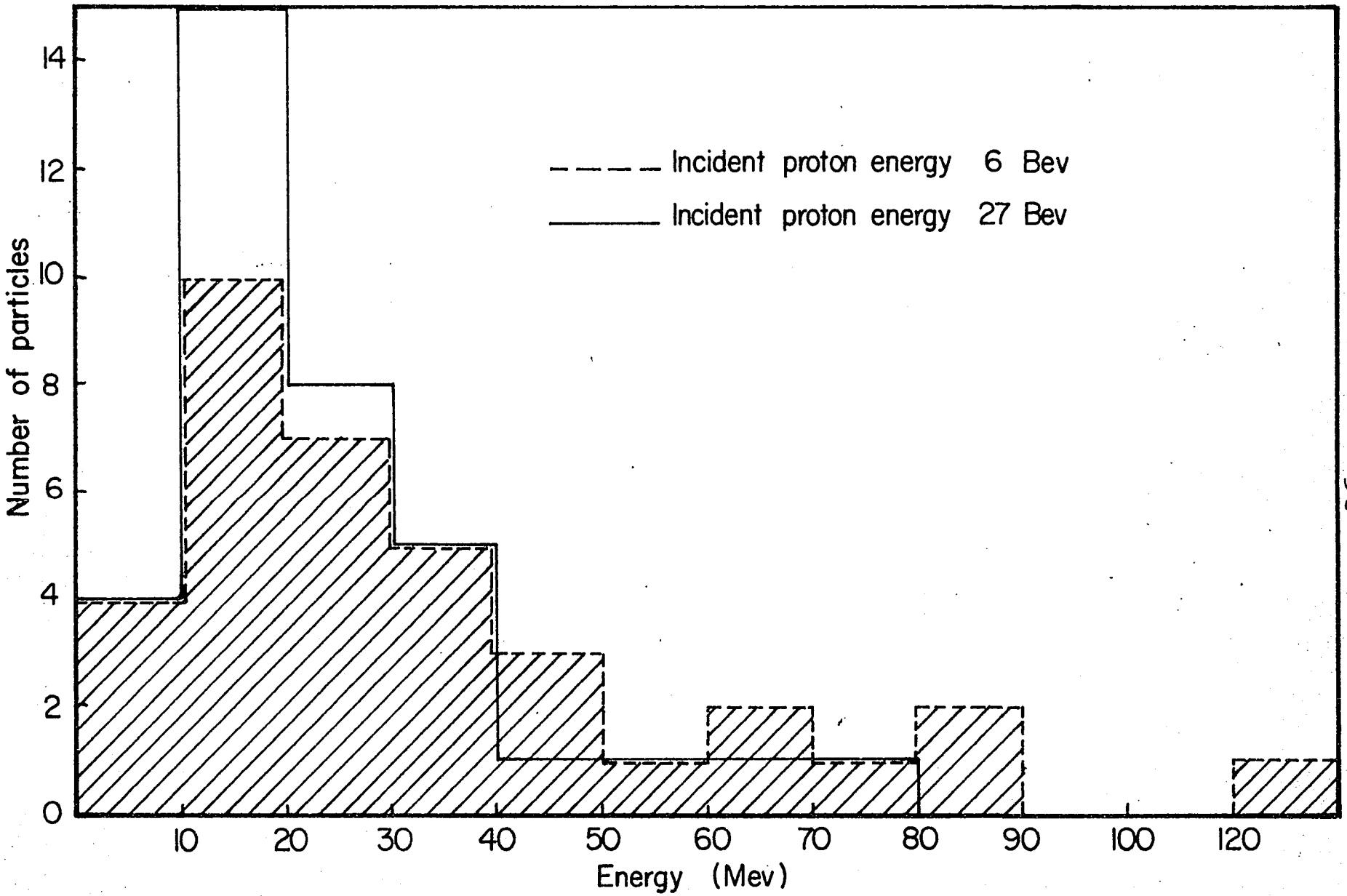

Fig. 22 Alpha particle energy spectra for stars with $n_b > 14$.

observations were used to apply a correction to account for the loss of the low energy particles (shown as shaded area on Figure 20). The mean energy of the α particles is found to be (24.3 ± 1.8) MeV and (23.0 ± 1.5) MeV for the 6 BeV and 27 BeV interactions respectively. If only the α particles with energy less than 30 MeV are considered, the values of the mean energy are reduced to (16.6 ± .8) MeV and (15.3 ± .7) MeV respectively.

The combined spectra for incident energies of 6 BeV and 27 BeV is compared with the results of (Harding, Lattimore and Perkins) and Page, in Figure 21 for α particle energies less than 30 MeV. The agreement is quite good.

Figure 22 shows the α energy spectra (normalized to the same number of tracks) for stars with more than 14 black tracks. The figure suggests a higher proportion of energetic particles at 6 BeV.

4. Comparison with Evaporation Theory.

i) Proton spectra.

The combined energy distribution for the 6 and 27 BeV interactions are shown in Figure 23. The maximum in the spectrum occurs at a value of E equal to 7-8 MeV, and the mean energy is ~ 11 MeV.

Using these values, the effective mean temperature, T, and barrier height V° are both found to be 3-5 MeV.

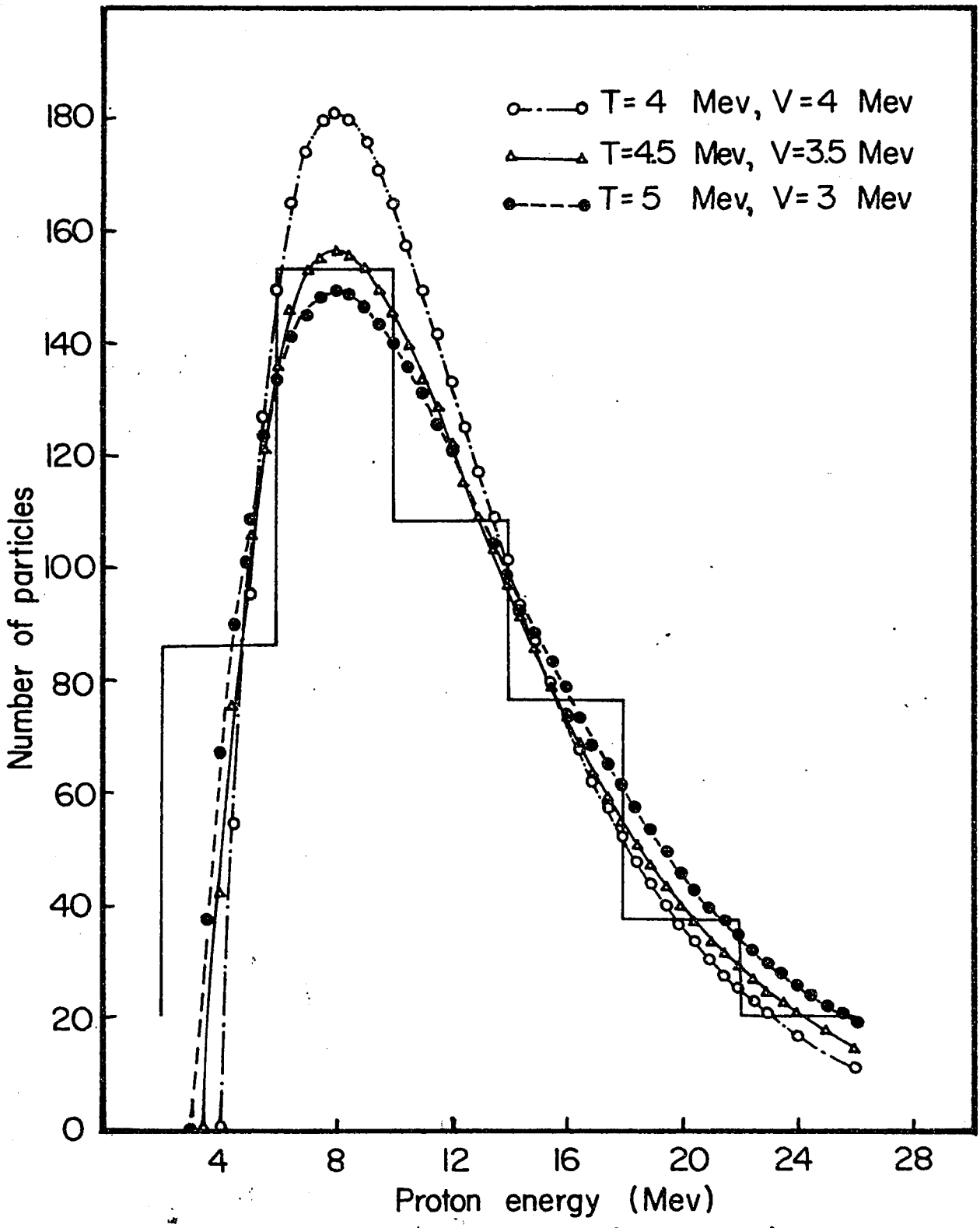

Fig. 23 Experimental and theoretical (normalized) energy spectra of evaporated hydrogen nuclei.

The values which give the best fit of the theoretical curve to the observed spectrum are also determined in the figure. The best values of the parameters are found to be:

$$T = 4.5 \text{ MeV} , \quad V = \sim 3.5 \text{ MeV}$$

It is to be noted that the energy spectra for singly charged particles was determined, assuming all of the particles to be protons. The value of the mean energy and effective temperature, taking into account the presence of deuterons and tritons, must therefore be ~ 20% higher than the indicated values.

Figure 18 indicates a slightly lower average energy of the protons observed in the interactions with an incident energy of 27 BeV, hence a lower temperature. This result is contrary to expectations, as theory predicts that the temperature should increase with increasing excitation energy ($U \sim aT^2$).

The comparison with theory is complicated by the fact that the nuclear temperature does not remain constant during the process, but falls as the evaporation proceeds. Further, as charged particles are emitted, the height of the Coulomb barrier decreases. Such effects will be more important, the greater the initial excitation energy. Increased fragmentation at 27 BeV could produce a substantial lowering of the excitation energy and barrier height, thus explaining the lower values of these parameters found at 27 BeV.

(ii) α Particle Spectra.

Since the α particle spectra at 6 BeV and 27 BeV are not significantly different, the combined spectrum can be used to make a comparison with theory. The spectrum is shown in Figure 24, where all curves are normalized at 15 MeV.

The expected theoretical curve for the evaporation of α particles corresponds to a value of the nuclear temperature, $T \sim 5$ MeV, and an effective barrier height ~ 11 MeV. The curve calculated for these parameters is in complete disagreement with the observed energy distribution (curve (a) in the figure).

The experimental energy distribution can only be explained by assuming an evaporation temperature higher than the binding energy of the nucleus. The theoretical curve for $T = 11$ MeV, $V' = 2$ MeV, is represented by curve (b) in the figure.

The necessity of invoking such a high nuclear temperature in order to explain the emission of the high energy particles makes it appear impossible to consider the emission of these particles as being due to an evaporation process from an equilibrium state.

If we consider only the part of the energy spectrum below 30 MeV (the energy above wich the theory of Le Couteur predicts very few evaporated α particles), partial agreement with evaporation theory is obtained. The maximum in the energy distribution is ~ 12 MeV and the mean energy is ~ 16 MeV (Fig. 25).

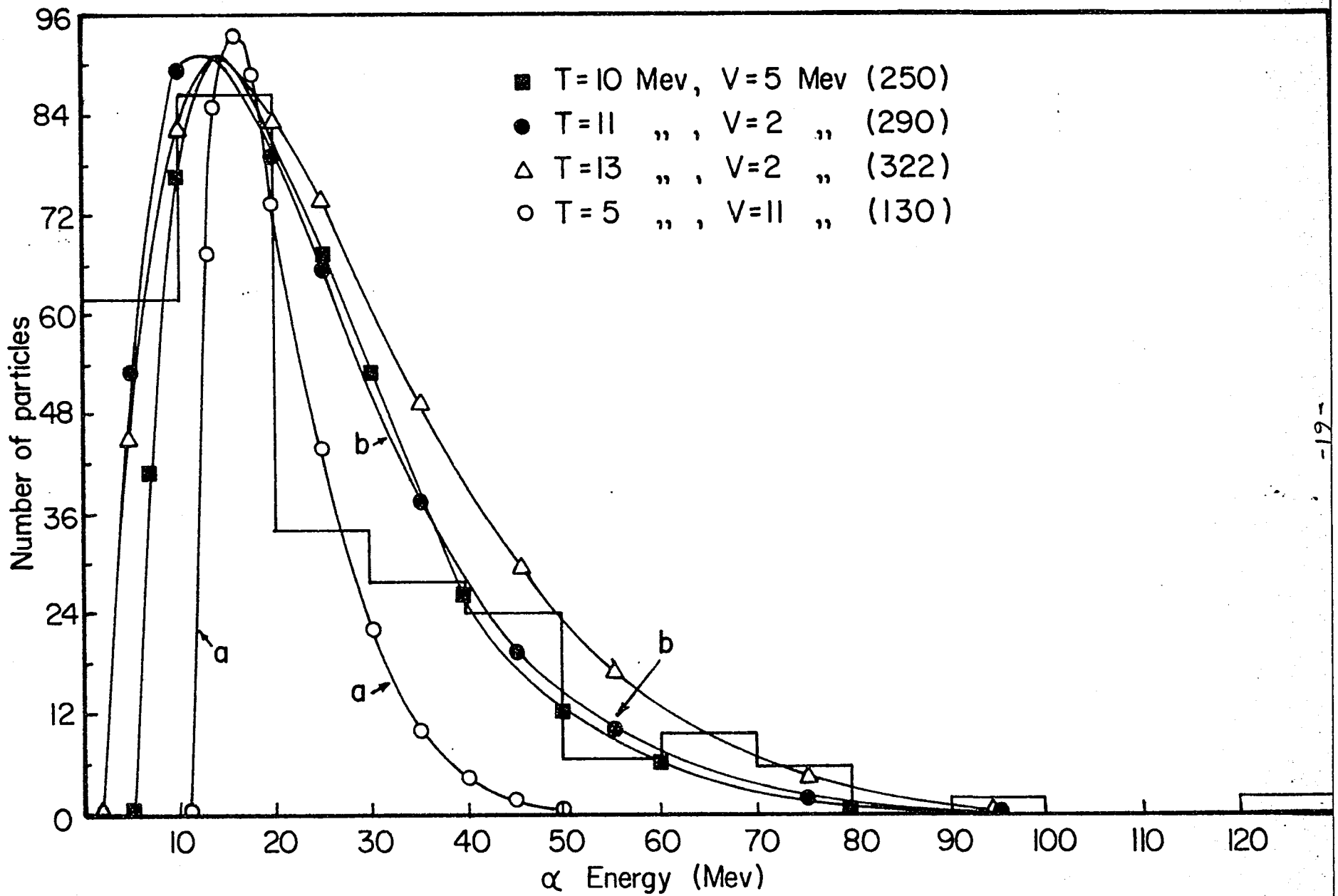

Fig. 24 Theoretical and experimental results for the energy spectrum of evaporated particles

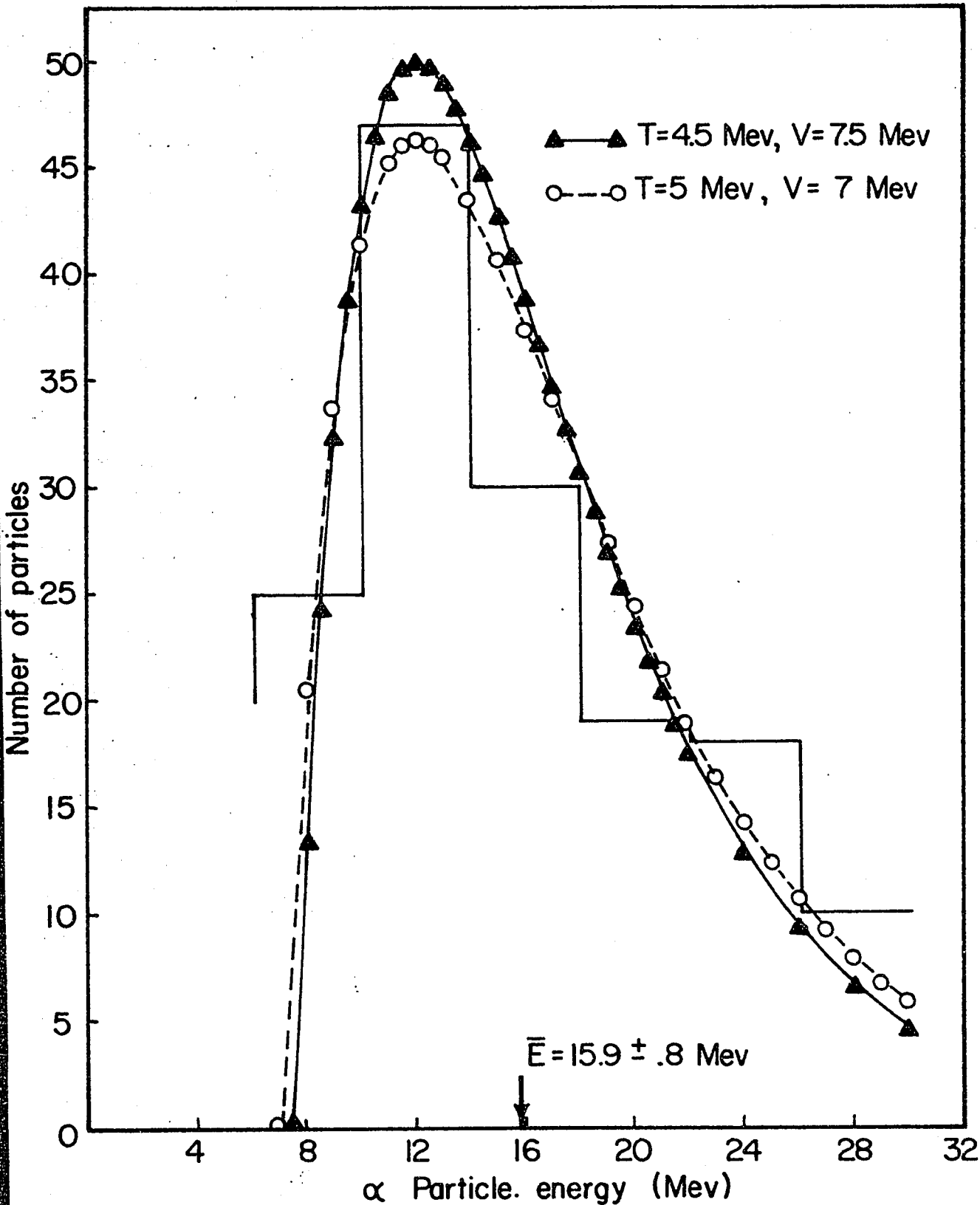

Fig. 25 Experimental and theoretical (normalized) energy spectra of evaporated helium nuclei for ($6 < E_\alpha < 30$) Mev.

This corresponds to a nuclear temperature of T ~ 4-5 MeV and an effective potential barrier V' ~ 8 MeV. The figure shows a satisfactory fit of the theoretical curves to the observed energy distribution using these values of the parameters T and V', except that it does not account for the emission of low energy α particles (E_α < 6 MeV).

(d) Emission Ratios.

1. Theoretical Predictions.

Calculations of the relative probabilities of emission of different types of particles have been made by Weisskopf. Le Couteur has modified Weisskopf's formula to take into account the effect of quantum mechanical penetration of the potential barrier. The theory of Le Couteur predicts the total number of evaporated particles, N, and the numbers of protons, deuterons, tritons and α particles emitted at different values of the excitation energy, U. The curves calculated by Le Couteur are shown in Figure 26 in which n_p and n_α refer to all the singly and doubly charged particles, respectively, since experimentally it is not usually possible to identify the particles within each of these groups.

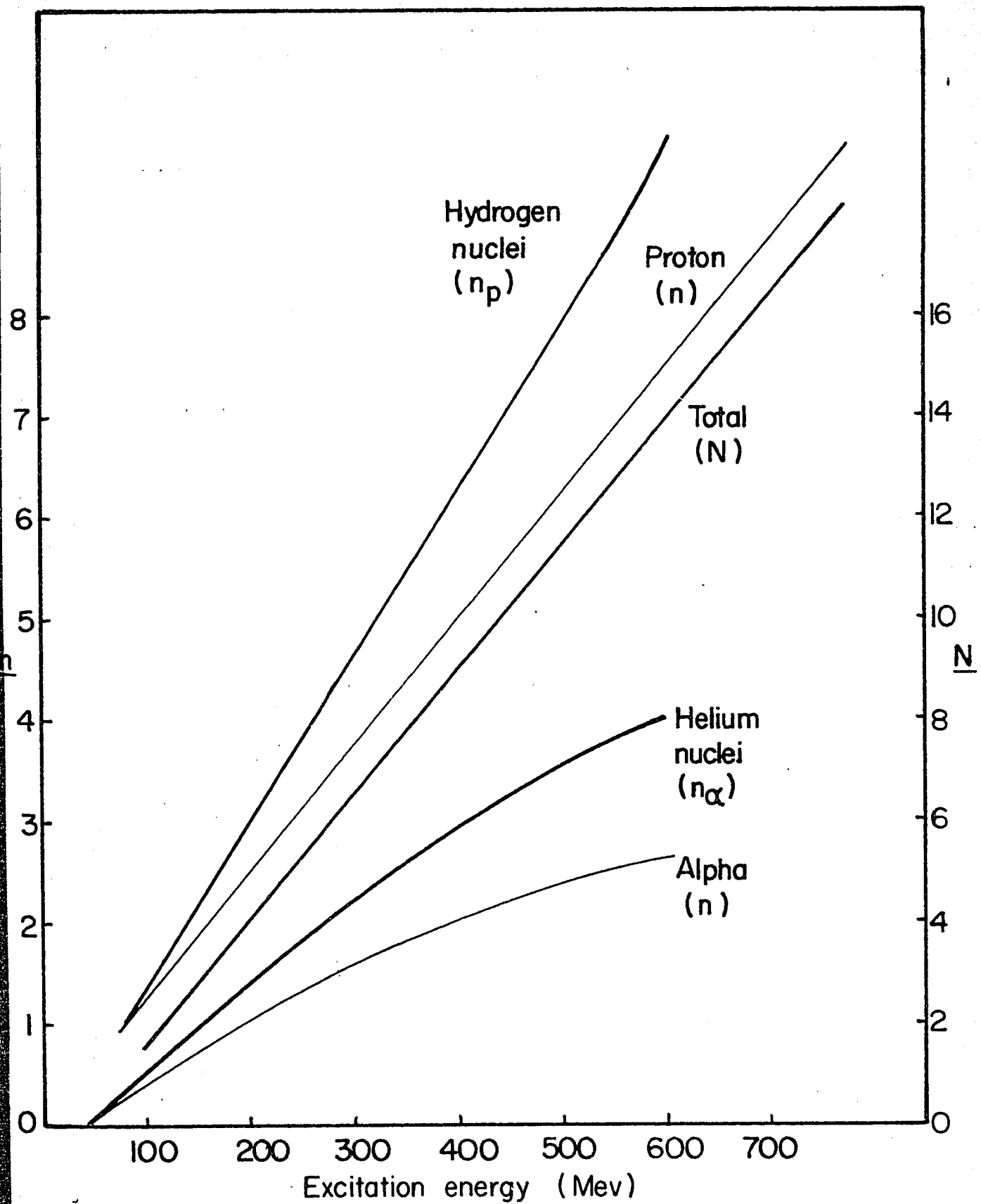

Fig. 26 Variation of emission of protons, alpha particles and total emission with excitation energy.

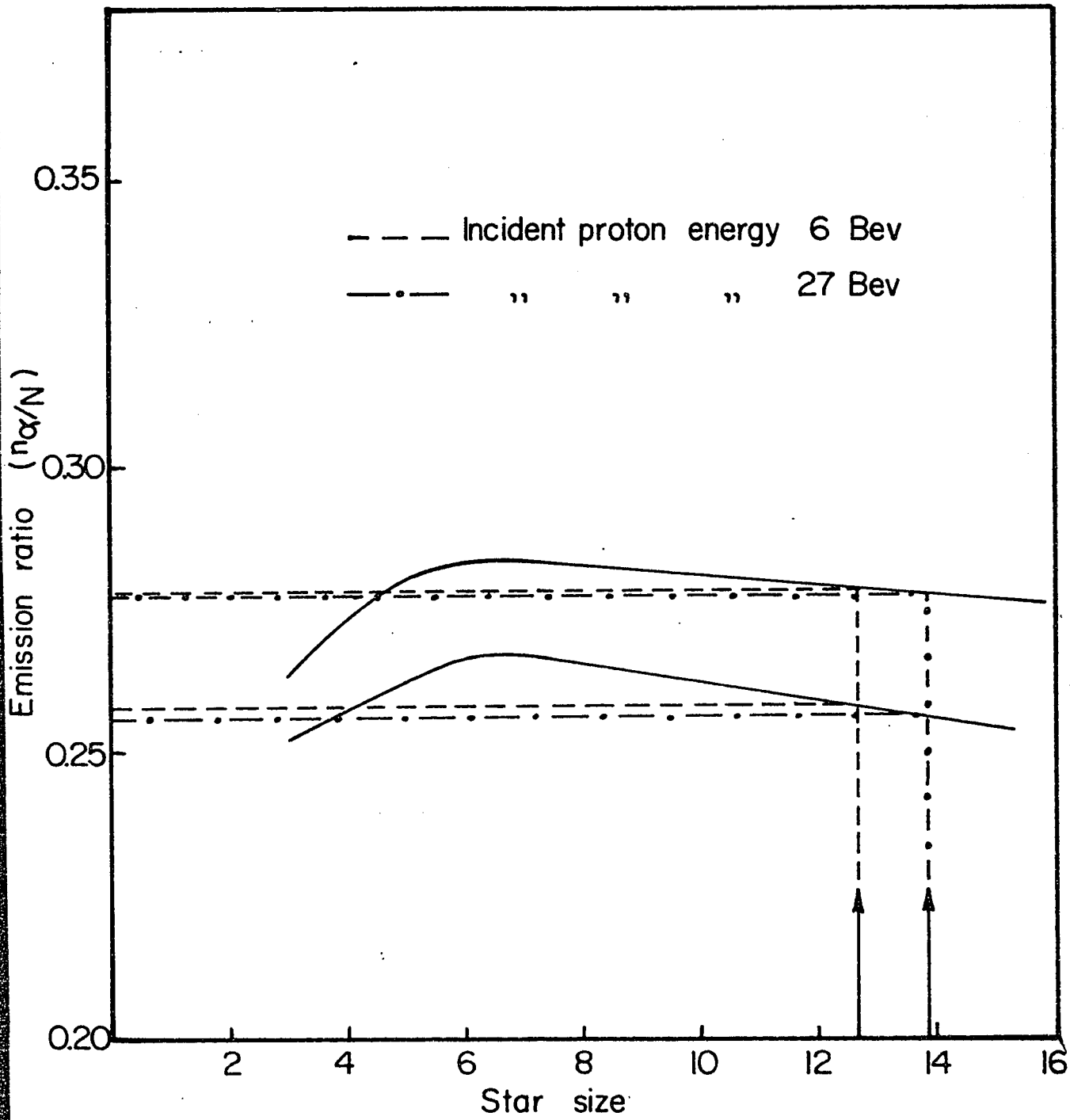

Fig. 27 Theoretical values of the emission ratio as a function of the star size.

Figure 27 gives the predicted emission ratio n_α/N as a function of the number of black tracks in the stars; the two curves correspond to the upper and lower limits of the values of n_α/N. These curves show that for stars with more than 7 black tracks, the calculated emission ratio decreases linearly with star size.

Theory predicts that the number of evaporated fragments should be very small ($\sim$ 1.5%).

2. Experimental Determination.

In this study a total of 718 tracks, coming from 96 stars, 52 at a proton energy of 6 BeV and 44 at a proton energy of 27 BeV, were used. The tracks selected had grain densities $g \geq 10\ g_o$, and made angles of dip $< 30^\circ$ in the unprocessed emulsion. The particles producing the tracks were identified, using the techniques described in Part I.

The results obtained for the emission ratio, n_α/N, for the two incident energies of 6 BeV and 27 BeV, were compared with the theoretical values calculated by Le Couteur. The results are shown in Table II.

Table II

Comparison of theoretical and experimental emission of α particles and fragments.

Incident proton energy	Average number of black tracks/star	n_α/N (theor.)	n_α/N (exptl.)	Percent fragments (theor.)	Percent fragments (exptl.)
6 BeV	12.7	.26 - .28	.32 ± .03	1.5%	1.5%
27 BeV	13.9	.25 - .28	.29 ± .03	1.5%	1.6%

The values of the emission ratio n_α/N in Table II do not include the particles of range < 30 μ. This range corresponds to a proton energy of ~ 1.5 MeV and an α particle energy of ~ 6 MeV. Due to the lower energy of the protons in the range interval of 0-30 μ, it is reasonable to assume a much higher proportion of α particles than protons for these low energy particles. In fact, the number of protons of range < 30 μ has been observed, in less sensitive emulsion, to be almost negligible[33]. The addition of the low energy α particles causes an increase in the emission ratio, indicated in Table III.

Table III

Determination of emission ratio n_α/N.

Incident proton energy	n_α/N theoretical	n_α/N corrected	n_α/N E_α < 30 MeV
6 BeV	.26 - .28	.34 ± .03	.27 ± .03
27 BeV	.25 - .28	.32 ± .03	.26 ± .03

3. Comparison with Theory.

The experimental values of the emission ratio for α particles are slightly higher than the calculated values. The theory of Le Couteur applies, however, only to the evaporated particles. The results obtained for the angular and energy distributions of the α particles have shown that the energetic α particles are probably emitted in the first stages of the interaction. The difference between the observed and calculated values is, therefore, probably due to the addition of the energetic α particles to the evaporated particles. If these energetic particles are omitted, the emission ratios fall within the limits of the predicted values as indicated in Table III.

In the case of the light fragments, the theory of nuclear evaporation predicts that about 1.5% of the particles evaporated from heavy nuclei should be fragments of charge $Z > 2$. The experimental results obtained at 6 BeV and 27 BeV are in agreement with the theoretical predictions, the values found being $\sim$ 1.5% for the two incident proton energies. However, the experimental emission ratios are probably too low, since tracks shorter than 30 μ were not identified and a large proportion of these tracks may be due to fragments.

III. DISCUSSION.

a. Proton Emission.

The lower average energy of the evaporated protons from the 27 BeV interactions compared with those at 6 BeV is surprising. One would have expected that the excitation energy at 27 BeV would have been greater than at 6 BeV, as indicated by the larger number of black prongs in the 27 BeV stars (an average of 13.9 black tracks per star compared with 12.7 prongs per star at 6 BeV). The average excitation energy in the two cases can be estimated approximately as follows:

	6 BeV	27 BeV
Average number of black tracks :	12.7	13.9
Emission ratio :	0.34	0.32
Number of protons :	8	9
Number of neutrons :	11	12
Number of α particles :	4	4
Number of fragments :	$\sim$ 1	1
Average kinetic energy of protons :	11.2 MeV	10.2 MeV
Average kinetic energy of α particles :	24.3 MeV	23.0 MeV
Binding energy of protons & neutrons :	8 MeV	8 MeV
Binding energy of α particles (inside the nucleus) :	4 MeV	4 MeV

Average excitation energy at 6 BeV = $(8 \times 19.2) + (11 \times 16) + (4 \times 28.3) + (1 \times 50)$ MeV $\approx$ 493 MeV.

Average excitation energy at 27 BeV = $(9 \times 18.2) + (12 \times 15) + (4 \times 27.0) + (1 \times 50)$ MeV $\approx$ 503 MeV.

The mean excitation energy per star appears to be practically the same for incident proton energies of 6 BeV and 27 BeV. The difference between the two observed spectra could, therefore, be explained as being due to statistical fluctuations in the number and energy of the evaporated particles, the nuclei being left with essentially the same excitation energy in the two cases.

It is interesting to note that:-

(i) the average excitation energy per star ($\sim$ 400 MeV) is only a small fraction of the energy of the incident particle:

- $<$ 7% at 6 BeV,
- $<$ 2% at 27 BeV.

(ii) the average excitation energy has increased very little (if at all) with an increase in the energy of the incident proton from 6 BeV to 27 BeV.

b. α Particle Emission.

The high temperature found for the α particle energy spectrum is consistent with similarly high temperatures found by other workers[15,16] for the energy spectra of heavier fragments. Such abnormally high temperatures ($\sim$ 11 MeV), which are greater than the binding energy per nucleon, are evidently not in agreement with evaporation theory.

The anisotropic angular distribution observed for the α particles of energies greater than 30 MeV indicates that these particles are not associated with the evaporation process, but are probably produced in the cascade. However, this does not account for the presence of the very low-energy α particles which can only be explained in terms of the evaporation theory by assuming a near collapse of the potential barrier, which becomes nearly equal to zero.

An explanation could be that at very high excitation energies (U $\sim$ 500 MeV), the process of evaporation from the nuclear surface occurs more rapidly than the equipartition of the excitation energy within the nucleus[1,29]. This effect could explain the emission of energetic α particles and fragments from "hot-spots" corresponding to abnormally high nuclear temperatures. At the same time an explanation would be provided for the emission of the very low-energy particles. When an energetic fragment escapes from the nuclear surface, the potential barrier suffers a strong deformation, resulting in a sudden lowering of the effective barrier height at this point. Nuclear particles (p, d, α) striking this region of the nuclear surface immediately after the emission of the fragment may escape from the nucleus although they have very low energies.

The angular distribution of the α particles indicates that the α particles of energy > 30 MeV are emitted predominantly in the forward direction, the forward/backward ratio being 3.5/1.

The same effect has been observed in the case of Li^8 and other heavier fragments. This effect can be explained on the basis of a collision occurring between a fast nucleon (from the cascade) and a group of nucleons (deuterons, α particles, etc.) which may exist instantaneously in the nucleus. A fast nucleon, colliding with such a "cluster" of nucleons close to the nuclear surface, will eject the particle, or fragment, in the forward direction. The emission of the fragments will be more forward the lower the energy of the incident particle; at 100 MeV incident energy a forward/backward ratio of 9/1 is observed for the light fragments, while at 10 BeV the ratio is only 2/1[34].

Perfilov[16] has calculated the number of α particles evaporated from a heavy nucleus for a bombarding energy of 100 MeV. The observed number of α particles emitted in the backward direction is found to be in agreement with the predictions of the evaporation theory. The excess of particles emitted forward can, therefore, be attributed to the collision of the incident proton with an α particle "cluster" near the nuclear surface. This effect could explain the asymmetrical angular distribution observed in the case of the energetic α particles.

PART III.

An Attempt to correlate the Distribution of Evaporated Particles with the π-Meson Multiplicity and Angular Distribution.

I. Introduction.

In previous studies by Ancsin[21] and by Lam[22], the inelastic collisions of 6 BeV protons with emulsion nuclei were analysed in terms of the angular distribution of the charged π-mesons produced in the interaction. It was observed that the interactions could be classified according to the effective target mass involved in the collision with the incident proton. The angular distributions of the charged π-mesons in the centre of mass system were found to be isotropic if three, four or five target nucleon masses (cascade type) were involved in the collision. However, in the case of collisions, involving a target mass of one nucleon, and also in peripheral types of collision with nucleons, it was found that the angular distribution in the centre of mass system did not show spherical symmetry.

Since the mechanism of emission of the low-energy particles may also depend on the type of initial interaction of the incident proton, it appeared to be of interest to compare the angular distributions of the black tracks in the cases of collisions involving:

(1) one target nucleon,

and (2) cascade type.

II. Experimental Techniques.

In this investigation, the black tracks were identified in 28 stars for which the charged π-meson angular distribution had already been determined. Out of these 28 events, 15 had been classified as interactions involving three, four or five target nucleons, the remaining 13 events corresponding to one target nucleon mass. The events studied were all large stars involving the emission of at least three charged π-mesons*.

These events had been studied in the Ilford G5 emulsion, previously used in Part I to compare various identification techniques. It had been found that the method of gap-counting gave good resolution between singly charged particles and those of higher charge, whereas track-width measurements resolved helium nuclei from the light fragments.

Using these techniques, an effort was made to identify all the black tracks in each of the 28 events. Approximately half of the tracks studied were steep tracks (angle of dip greater than 30°), for which the identification is difficult.

*In addition to these 28 stars, Ancsin and Lam studied the π-meson distribution in another 40 events. These stars, not included in the present study, correspond to cases in which less than three charged mesons are emitted. These interactions could involve the emission of a high proportion of neutral mesons, although in about half of the events the emission of steeply-inclined tracks might account for the mesons not having been identified.

A series of tracks were studied and grouped according to their angle of dip in the emulsion. Each group consisted of tracks with an angle of dip varying within a range of ten degrees. In each group the tracks were compared in terms of the δ-ray density and track width. In each case it was found that most of the tracks fell into two main groups, corresponding to lighter and heavier particles, which were identified as hydrogen nuclei and helium nuclei. The remaining tracks were considered to be due to light fragments, on account of their δ-ray density and larger track width. Some of the very steep tracks were classified as unidentified, as no useful measurements could be obtained. Although the identification of the steep tracks was more subjective than in the case of the flat tracks, the techniques used were considered sufficiently good to allow a comparison to be made of the interactions involving different target masses.

III. Experimental Results.

In the 28 stars studied, a total of 320 black tracks were identified. The classification of these tracks for the two types of interaction mentioned is shown in Table IV.

The number of black tracks per star is 13.3 and 9.2 for the interactions involving (3 - 4 - 5N) and (1N) target masses, respectively.

Table IV

Classification of black tracks.

Target mass	No. of stars	No. of black tracks	Protons	Alpha Particles	Fragments	Unidentified
3-4-5N	15	200	141	38	7	14
1N	13	120	73	29	9	9

Table V

Relative abundances of classified black tracks.

Target mass	Protons	Alpha Particles	Fragments	Unidentified
3-4-5N	70.5%	19%	3.5%	7%
1N	61%	24%	7.5%	7.5%

Table VI

Forward to backward ratio (F/B) for blacktracks, protons and alpha particles.

Target mass	F/B for black tracks	F/B for protons	F/B for alpha particles
3-4-5N	1.6 ± .3	1.8 ± .2	.90 ± .2
1N	1.1 ± .1	1.3 ± .2	.93 ± .2

Table V gives the relative abundances (as a percentage of the total number of particles emitted) of particles of charges $Z = 1$, $Z = 2$ and $= Z > 2$. In each group of stars, $\sim 7\%$ of the black tracks were unidentified.

The angular distributions of the black tracks and the singly and doubly charged particles for the two classes of interaction are shown in Figures 28, 29 and 30, respectively. The forward/backward ratio, F/B, for each of these distributions is given in Table VI.

IV. Discussion.

Due to the poor statistics, it is difficult to make a serious comparison between the two types of interaction, (p - 1N) and (p-cascade). Moreover, a comparison with the stars analysed in Part II is unreliable, as the method of analysis used in the latter case was different. Only about one-half of the tracks was studied in this case, owing to the rejection of short tracks ($R < 30\ \mu$) and tracks having angles of dip $> 30^{\circ}$. Nevertheless, certain tentative conclusions may be drawn.

(a) Comparison of Numbers of Black Prongs.

(1) (p - 1N) interactions: $\bar{N}_b = 9.2$

(2) (p - cascade) interactions: $\bar{N}_b = 13.3$

(3) All stars ($N_b \geq 8$): $\bar{N}_b = 13.3$

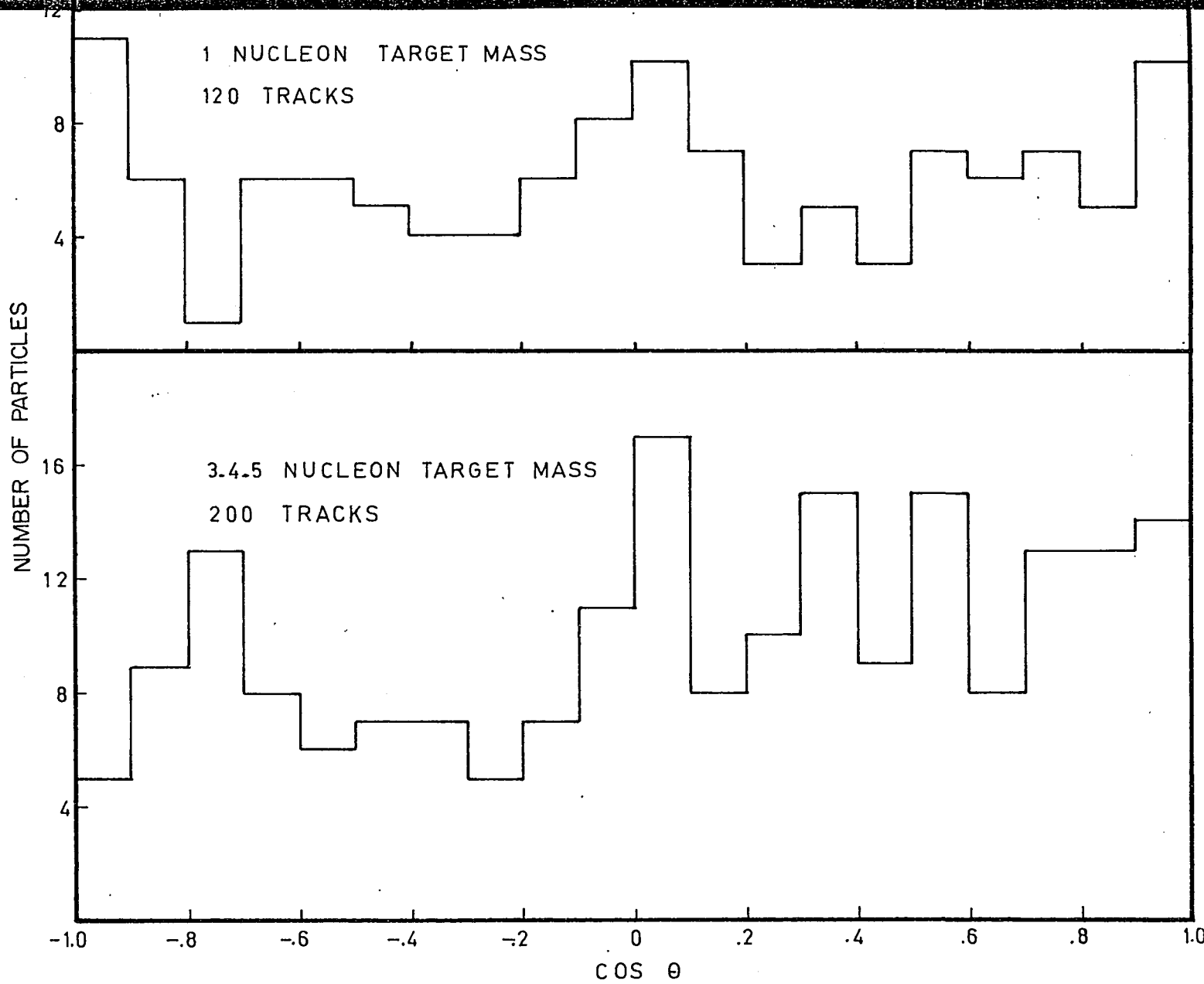

FIG. 28 ANGULAR DISTRIBUTION OF THE BLACK TRACKS EMITTED FROM THE INTERACTION OF 6 BeV PROTONS WITH DIFFERENT "TARGET MASSES" IN Ag+Br NUCLEI.

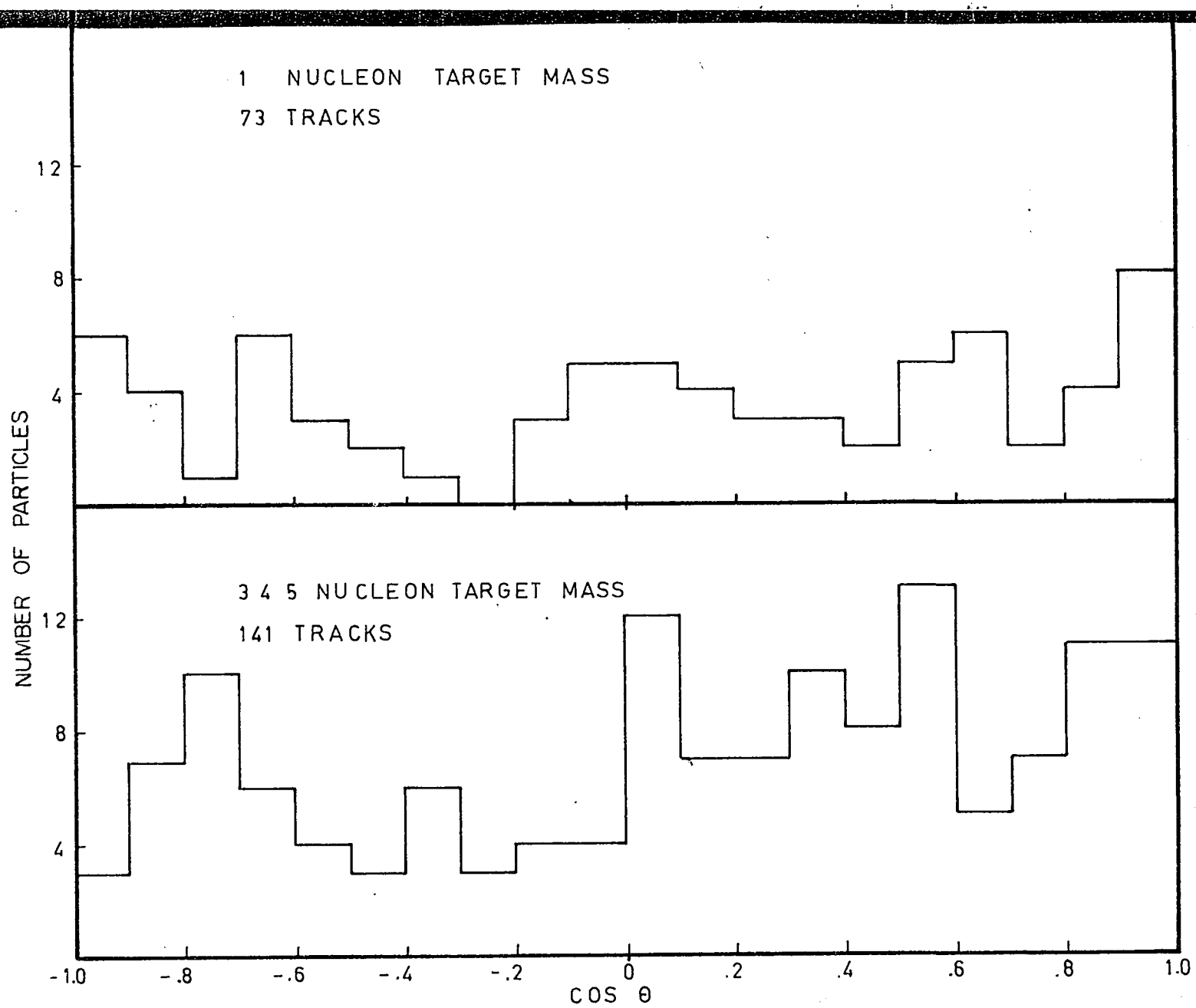

FIG. 29 ANGULAR DISTRIBUTION OF THE PROTONS EMITTED FROM THE INTERACTION OF 6 BeV PROTONS WITH DIFFERENT "TARGET MASSES" IN Ag+Br NUCLEI.

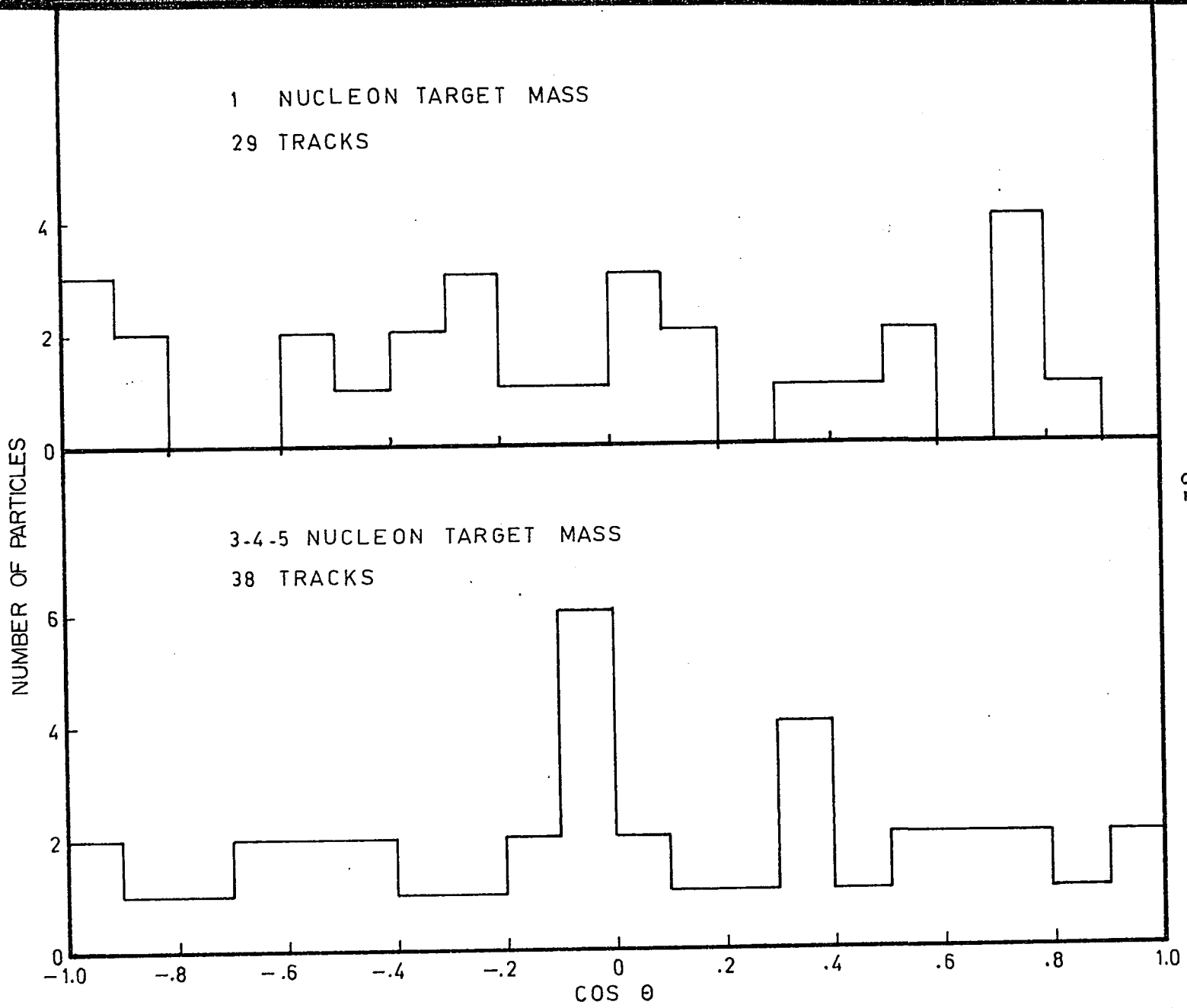

FIG. 30 ANGULAR DISTRIBUTION OF ALPHA PARTICLES EMITTED FROM THE INTERACTION OF 6 BeV PROTONS WITH DIFFERENT "TARGET MASSES" IN Ag+Br NUCLEI.

From these data we can estimate the average number of black tracks in the 40 events which were not identified as clear cases of either (p - 1N) or (p - cascade) interactions as follows:

$$13 \times \bar{N}_b^{(1N)} + 15 \times \bar{N}_b^{(\text{cascade})} + 40\ \bar{N}_b^{(\text{unidentified})} = 68 \times \bar{N}_b^{(\text{total})}$$

$$\bar{N}_b^{(\text{unidentified})} = \frac{68 \times 13.3 - [13 \times 9.2 + 15 \times 13.3]}{40}$$

$$= 15.1$$

These stars, which seem to be those with the largest average number of black tracks, correspond to more complex interactions in which either the created mesons produce secondary collisions inside the nucleus, or a high proportion of neutral mesons are produced, thus making impossible the analysis of the event from the observed charged meson angular distribution. Thus, we can conclude that on the whole, the stars corresponding to (p - 1N) or (p - 3N - 4N - 5N) interactions are smaller than the stars for which the centre-of-mass does not correspond to one of these groups. One should also take into account a certain number of stars corresponding to peripheral collisions with nucleons of the target nucleus. The majority of these events were found to be amongst the small stars ($N_b < 8$), which were not included in the events classified as interactions with silver and bromine nuclei. Only three or four interactions of

this type were identified in the large stars ($N_b \geq 8$). This could imply that a peripheral type of collision is improbable when the interaction occurs with a nucleon in the interior of the nucleus, the peripheral interactions occurring mainly with a nucleon on the periphery of the nucleus.

(b) Emission Ratio, $^{n}\alpha/N_b$.

(a) (p - 1N) interactions	:	$^{n}\alpha/N_b = 0.24 \pm 0.05$
(b) (p - cascade) interactions	:	$^{n}\alpha/N_b = 0.19 \pm 0.03$
(c) All stars ($N_b \geq 8$)	:	$^{n}\alpha/N_b = 0.33 \pm 0.03$

The ratio, $^{n}\alpha/N_b = 0.33 \pm 0.03$, found for all the stars is somewhat high compared with the theoretical value of ~ 0.26*. However, in the case of the smaller stars ($\bar{N}_b = 9$), corresponding to (p - 1N) collisions, the emission ratio, $^{n}\alpha/N_b = 0.24 \pm 0.05$, is in good agreement with the value calculated from evaporation theory for an evaporation temperature T of 4 - 5 MeV. The most surprising case is that of the stars resulting from a cascade (p - nN), for which the ratio is found to be 0.19 ± 0.03. This value, however, may not be significantly different from the ratio found for the one-nucleon interactions, as the values agree within the limits of the statistical errors.

*This higher ratio can be explained by the presence of cascade α particles, as indicated by the α particle angular distribution.

Le Couteur's calculations show that an emission ratio of about 0.19 would be consistent with a higher excitation temperature, T, and an appreciable lowering of the effective barrier height, V'.

These results tend to indicate that the one-nucleon interactions of the type $p + N \rightarrow 2N + n\pi^{\pm}$ give less excitation energy to the nucleus than the cascade interactions. The single nucleon interactions correspond to a collision of the incident proton with a nucleon most likely at the periphery of the nucleus. The two nucleons, being close to the nuclear surface, leave the nucleus without suffering any further inelastic collisions. An important factor, which can contribute to the increase of the ratio n_{α}/N_b in the case of peripheral collisions is that the angular momentum acquired by the nucleus can be more easily dissipated by the emission of a fragment, α, Li, etc., than by the emission of a nucleon. An interesting result which corroborates this hypothesis is that the percentage of fragments emitted in the one-nucleon interactions is $\sim 7.5\%$, whereas in the case of the stars corresponding to interactions of the type (p - cascade), the percentage of fragments is $\sim 3.5\%$.

(c) Angular Distributions.

The isotropic distributions observed for the α particles is in agreement with evaporation theory. This result corroborates the hypothesis that the forward emission of α particles is largely associated with more complex interactions, involving a larger number of target nucleons, the energetic α particles emitted forward being produced as the result of interactions provoked by the cascade.

The forward peaking observed in the proton angular distribution in the case of (p - cascade) interactions indicates that the proton suffers a head-on collision in which nucleons, projected in the forward direction, may escape from the nucleus without undergoing further collisions. The almost isotropic distribution observed in the case of the (p - 1N) interactions seems to indicate that these collisions are mainly edge-on collisions, giving the nucleus a large angular momentum. Emission of fragments should then be favoured. In spite of the poor statistics, the results indicate a higher proportion of fragments from the (p - 1N) interactions, in agreement with this hypothesis.

CONCLUSION:

The results of this work seem to indicate that there is very little difference in the excitation energy produced in Ag and Br nuclei by 6 BeV protons and 27 BeV protons. The only observed difference, in the two types of interaction, is a slightly stronger forward peeking and higher frequency of energetic α particles at 6 BeV. This tends to support the hypothesis that the "tunnel" produced by the incident particle, when traversing the nucleus, is "cleaner" at higher incident particle energies.

It has been shown that the black tracks emitted as a result of interactions of 6 BeV and 27 BeV protons with Ag and Br nuclei cannot be explained solely in terms of evaporation theory. It is suggested that "hot spots" produced at the nuclear surface may be responsible for the emission of energetic particles before an equilibrium state is reached. A possible explanation for the emission of abnormally low energy α particles and protons is based on a proposed partial collapse of the Coulomb potential barrier upon emission of a charged particle ($Z \geq 2$). If a proton or α particle strikes this region of the nuclear surface, before restoration of the Coulomb barrier, it could possibly escape with an energy much lower than the energy corresponding to the height of the Coulomb barrier.

Other mechanisms, such as the collision of energetic nucleons with nuclear "clusters" near the surface of the nucleus, and processes of absorption and emission of mesons, may contribute

to the emission of particles prior to the evaporation from the thermodynamic equilibrium state.

BIBLIOGRAPHY

(1) J. B. Harding, S. Lattimore and D. H. Perkins, Proc. Roy. Soc. 196, 325 (1949).

(2) D. H. Perkins, Phil. Mag. 40, 601 (1949).

(3) D. H. Perkins, Phil. Mag. 41, 138 (1950).

(4) N. Page: Proc. Phys. Soc. A63, 250, 1950.

(5) P. E. Hodgson, Phil. Mag. 42, 83 (1951).

(6) P. E. Hodgson, Phil. Mag. 43, 934 (1952).

(7) P. E. Hodgson, Phil. Mag. 44, 1113 (1953).

(8) P. E. Hodgson, Phil. Mag. 45, 190 (1954).

(9) S. O. C. Sorensen, Phil. Mag. 42, 188 (1951).

(10) J. Crussard, Thesis, Paris (1952).

(11) V. I. Ostroumov, J. Exptl. Theoret. Phys. (U.S.S.R.) 32, 3 (1957); Soviet Phys. JETP 5, 12 (1957).

(12) V. M. Sidorov and E. L. Grigoriev, J. Exptl. Theoret. Phys. (USSR) 33, 1179 (1957); Soviet Phys. JETP 6, 906 (1958).

(13) P. A. Vaganov and V. I. Ostroumov, J. Expt. Theoret. Phys. (USSR) 33, 1131 (1957); Soviet Phys. JETP 6, 871 (1958).

(14) E. W. Baker, S. Katcoff and C. P. Baker, Phys. Rev. 117, 1352 (1960).

(15) N. A. Perfilov, N. S. Ivanova, O. V. Lozhkin, M. M. Makanov, V. I. Ostroumov, Z. I. Solov'eva and V. P. Shamov, J. Exptl. Theoret. Phys. (USSR) 38, 345 (1960); Soviet Phys. JETP 11, 250 (1960).

(16) R. Arifkanov, M. M. Makanov, N. A. Perfilov and V. P. Shanov, J. Exptl. Theoret. Phys. (USSR) 38, 1115 (1960); Soviet Phys. JETP 11, 806 (1960).

(17) R. M. Kalbach, J. J. Lord and C. H. Tsao, Phys. Rev., 113, 330 (1959).

(18) R. R. Daniel, R. N. Kameswara, P. K. Kalhotra, Y. Tsuzuki, Nuovo Cimento, 16, 1 (1960).

(19) F. M. Friedländer, Nuovo Cimento, 14, 796 (1959).

(20) A. Barbaro-Galtieri, A. Manfredini, B. Quassiati, C. Castagnoli, A. Garnotti, and Ortalli, Nuovo Cimento, 21, 469 (1961).

(21) J. Ancsin, Thesis, University of Ottawa (1961).

(22) S. T. Lam, Thesis, University of Ottawa (1962).

(23) V. F. Weisskopf, Phys. Rev. 52, 295 (1937).

(24) K. J. Le Couteur, Proc. Phys. Soc., A63, 259 (1950).

(25) M. Blau, A. R. Oliver and J. E. Smith, Phys. Rev. 91, 949 (1953).

(26) B. Judek, Nuovo Cimento, 16, 834 (1960).

(27) J. E. Hooper, E. Dahl-Jensen and E. B. Neergaard, Nuovo Cimento, 15, 211 (1959).

(28) H. Fay, K. Gottstein and K. Hain, Nuovo Cimento, 11, 234 (1954).

(29) Y. Fujimoto and Y. Yamaguchi, Prog. Theor. Phys. 4, 468 (1948).

(30) S. Tomonaga, ZS f Physics, 110, 573 (1938).

(31) C. M. Lattes, P. H. Fowler and P. Cüer, Proc. Phys. Soc. 59, 883 (1947).

(32) W. H. Barkas, F. M. Smith, H. Bradner and A. S. Bishop, Phys. Rev. 77, 462 (1950).

(33) J. Hébert and J. Hébert, Annales de l'ACFAS, (1963).

(34) Perfilov, N. A. - Proceedings of the the International Conference on High Energy Physics and Nuclear Structure - CERN 63-28, July 1963.